NASA
Ames Research Center

Report No. WR-001
Date 12-31 90
Prep. by Rose Enger
Page of

System Engineering Report

Sofia Wind Tunnel Data Analysis & Implications
SUBJECT PROJECT
for the Full-Scale Sofia Aircraft
DISTRIBUTION

SOFIA WIND TUNNEL DATA ANALYSIS

AND IMPLICATIONS FOR THE FULL-SCALE SOFIA AIRCRAFT

31 December 1990

ROSE ENGINEERING & RESEARCH, INC.

P.O. Box 5146

Incline Village, Nevada 89450

SOFIA WIND TUNNEL DATA ANALYSIS
AND IMPLICATIONS FOR THE FULL-SCALE SOFIA AIRCRAFT

By

WILLIAM C. ROSE and JAMES M. COOLEY

Prepared for

SVERDRUP TECHNOLOGY, INC.

NASA-Ames Research Center

Moffett Field, CA 94035

Under Prime Contract NAS2-12940

31 December 1990

ROSE ENGINEERING & RESEARCH, INC.

P.O. Box 5146

Incline Village, Nevada 89450

I. BACKGROUND

NASA's Ames Research Center has operated the Kuiper Airborne Observatory (KAO) for the past fifteen years. During this time period, the feasibility and success of high altitude observatories for infrared and visible astronomy have been demonstrated. The KAO contains a 0.9 meter telescope that currently limits its use. A new, larger, 2.5 meter telescope in an airborne platform has been planned. The Stratospheric Observatory for Infrared Astronomy (SOFIA) will use a large telescope operating from a high altitude aircraft in a manner similar to that of the KAO.

NASA-Ames Research Center has conducted efforts in-house and through contractor personnel to provide studies into the design of the telescope, aircraft modification and installation in a large aircraft. Due to the size of the telescope system, the Boeing 747 has been tentatively identified as the candidate aircraft. The "SP" model of the 747 is a highly desireable version because of its performance characteristics and size.

Because of the requirement for infrared observation, the cavity containing the telescope will be required to be open during observations, that is no material window between the atmosphere and the telescope can be used. The aircraft would be expected to fly astronomical missions at operating altitudes between 40,000 and 45,000 feet above sea level. The environment within the telescope cavity must remain relatively benign to effectively carry out astronomical observations. In addition, because of the interest in visible astronomy that the facility is expected to support in addition to the infrared, the quality of obtained images must be made as good as possible within practical constraints.

Historically, the quality of the aerodynamic flow within and over an open cavity containing a telescope system has been of interest at the Ames Research Center for the past 20 years. Fundamental findings from several tests as they apply to the SOFIA aircraft are discussed here. The most profound aerodynamic phenomenon that may occur when air flows over and within an open cavity at the expected operating aircraft conditions is cavity resonance. Cavity resonance is characterized by the presence of ordered, single frequency pressure variations, usually within the acoustic domain. Harmonics of these single frequencies may also occur and multiple modes of resonance within a given cavity are possible, depending on the aerodynamic conditions. If resonance occurs and it remains uncontrolled, the pressure fluctuations can cause unwanted vibrations of the optical components within the cavity and cause degradation of the optical performance. In addition, structural effects or degradation caused by an uncontrolled resonance are potentially harmful and must be avoided at all cost. Previous wind tunnel experiments and flight tests have been carried out to examine the control of cavity resonance. Once the ordered cavity resonance is eliminated, conditions that exist in the cavity and on the fuselage in the areas surrounding the cavity may still contain substantial unwanted pressure variations, even though the cavity may not be resonating. Both conditions within the cavity and conditions on the remainder of the aircraft as a result of the presence of the open cavity are of interest in developing a flow control technique for any aircraft. This particular area of interest is known as aero-mechanical control, and much of the work done at NASA-Ames has been in this area.

Another topic of equal importance as aero-mechanical control is the issue of aero-optical control. Aero-optical control has to do with tailoring the aerodynamic flow field properties such that the image quality of any telescope system viewing through that flow field is as good as possible. The aero-optical issues concern themselves with the wavefront error induced by variations in the index of refraction that occur in the aerodynamic flow fields over and within the cavity. The time characteristics of the unsteady index-of-refraction field are tied to those of the unsteady (turbulent) aerodynamic density field. The turbulence produces high frequency (small-scale) aberrations that scatter light at large angles from the incident parallel rays, producing a reduction of the focal plane spot intensity, and can lead to large increases in the originally diffraction-limited spot size. On the other hand, lower frequency variations in the aerodynamic field produce tilts to the wavefront that move the image within the focal plane. Both of these aero-optical considerations limit the resolution of distant targets, which is an important consideration in the design and performance evaluation of the SOFIA aircraft.

Both the aero-mechanical and aero-optical issues have been investigated extensively in wind tunnel studies. However, when considering a potential SOFIA telescope installation in a 747-SP, the flow field in the area of the proposed cavity is not accurately represented by previous two-dimensional experiments and full-scale data from the KAO. Thus, a test of the proposed 747 model was required to investigate the flow over the 747 forebody.

Issues known to affect the performance of open cavity flows are the ratio of the upstream boundary layer thickness to cavity length, the nature of the three-dimensional flow field, and regions of potential pressure gradients, both streamwise and cross-stream, in the region of the open cavity. Because of these features, a wind tunnel test was proposed early in the SOFIA program to investigate the 747 forebody flow field. A wind tunnel model was tested from March to July 1990. Results of this testing are the subject of this report.

II. INTRODUCTION

The aerodynamic flow field over the Stratospheric Observatory for Infrared Astronomy (SOFIA) will determine many of the operating characteristics of the aircraft as a high altitude platform and observatory. The flow field is fully three-dimensional over the area proposed for the telescope cavity, which is downstream of the wind screen and just upstream of the wing-body fairing junction. On the 747-SP (the preferred aircraft) in the current concept the forward bulkhead is located at Station 520, while the downstream bulkhead is located at Station 700. The three-dimensional flow field arises primarily due to the upwashing velocity vector field forward of and above the low wing arrangement on the 747 aircraft. In addition to this three-dimensional flow field, the relative initial boundary layer thickness is small because the distance of the cavity from the origin of the fuselage's boundary layer on the 747 is not substantially longer than that on the KAO. However, when considering the large streamwise aperture required to accommodate the full 2.5 meter proposed SOFIA telescope, the ratio of upstream boundary layer thickness to cavity length is in a domain not previously investigated either on wind tunnel models or in flight. In addition to these two concerns, because of the complex nature of the 747 forebody and its interaction with the wing pressure field, both streamwise and transverse pressure gradients are expected to exist over any open aperture in the proposed area on the fuselage.

Any model that is designed to investigate the SOFIA flow field and the resulting optical implications of the aerodynamics must be large enough to obtain meaningful measurements of all of the parameters that can affect the overall performance. An initial concern is the existence of a facility to test a large enough model of the proposed

vehicle. The wind tunnel selected for the SOFIA test program was the NASA-Ames 14 x 14-ft transonic wind tunnel. This tunnel has been used extensively in previous aero-mechanical and aero-optical investigations, and the characteristics of the tunnel are well-known. The tunnel is relatively large and can accommodate a model of up to approximately 3 to 3½% blockage (of the test section area) without incurring substantial flow angularity and other flow non-uniformity to the external flow that might invalidate any test results. The range of Mach numbers for the test was chosen to be between 0.63 and 0.88, encompassing the normal operating Mach number of the 747-SP range between approximately 0.82 and 0.86 at altitudes of interest, and most of the conditions associated with descent and landing, which might have to be performed with the door open.

Given the maximum size restrictions for blockage in the 14-ft wind tunnel, and in order to bring the highest level of credibility to the test results, it was decided to use the largest possible model of the 747 forebody and wing arrangement. If a 747 model having full wings were used, the fuselage diameter and resulting boundary layer and shear layer characteristics would be smaller than those of the clipped-wing model that was finally decided upon. This model is a 7% scale model with the external section of the wings beyond the inboard engine nacelle-pylon group removed. The model was designed and fabricated by MicroCraft Corporation of Tullahoma, Tennessee. The model could be configured as either a 747-200 or a 747-SP version of the Boeing 747 aircraft. In the present study only the SP version was tested since it is the version of choice for the SOFIA platform and a viable solution for that platform was demonstrated in the test described here. The model incorporated a properly scaled version of the 2.5 meter telescope, along with various techniques for positioning the telescope and aperture at

different elevation angles. The model was delivered to NASA-Ames in June of 1989 and installed in the 14-ft tunnel in December of 1989. The model was mounted to the sting in the wind tunnel in order to be free of wall effects in the test section and to facilitate angle of attack and side slip variations. Because of questions concerning the validity of using a clipped-wing configuration, CFD analyses were performed by NASA personnel which showed that increasing the normal cruise angle of attack by about a half a degree compensates for the changes in local flow angularity in the region of the cavity brought about by the removal of the outboard wing sections.

The overall test objective for the present study was to provide design and off-design information on the ability of proposed shear layer control systems to eliminate cavity resonance and to develop a concept which could provide a benign cavity environment with acceptable aero-mechanical and aero-optical performance. With a functional anti-resonance system, the remaining design risk for the program will be reduced significantly. To do this, the cavity volume was modeled with scaled internal dimensions that represent the proposed flight article. A model of the telescope that simulates its gross volumetric features was mounted in the cavity. In order to control the shear layer, several flow control devices were designed and fabricated prior to the test. These control devices are attachments that can be mounted either ahead or downstream of the aperture, such as porous fences similar to the one currently used on the KAO. Other devices are aft ramps of varying depths, angles, and lengths.

The surface of the model was instrumented with several steady-state and unsteady static pressure sites. Within the cavity, several unsteady pressure transducers were

mounted to monitor the aero-mechanical performance of candidate flow control devices. During the aero-optical portion of the test, a moveable probe drive was used to place steady-state pitot and static pressure instrumentation at locations within the shear layer over the open cavity. This drive replaced the telescope model in this portion of the test and maintained the effective blockage of the telescope by incorporating a skirt around the drive. The instrumentation could be placed at selected locations within the aperture for all elevation angles. In addition to the steady-state probes, unsteady instrumentation (hot films) was mounted on the rake for determining the relevant turbulence information.

The NASA-Ames 14-foot tunnel operates with atmosphere (sea level) total pressure, so that the test section conditions vary substantially with Mach number. Mach numbers were chosen for this study to encompass a wide range of flow conditions, including the expected cruise range proposed for astronomy operations. The specific Mach numbers are 0.63, 0.70, 0.79, 0.82, 0.85 and 0.88. The value of 0.85 was chosen as a representative cruise condition and much of the information obtained in the test was for this Mach number. Similarly, angles of attack were chosen to encompass a wide range, with the cruise value chosen to be 2.5 degrees. One side slip angle (wind into the open cavity) of 4 degrees was tested. The cruise conditions (M = 0.85, α = 2.5 degrees, β = 0 degrees) were supplemented with others to ensure a useful margin of operation at other conditions. The wind tunnel cruise conditions resulted in a dynamic pressure of 660 psf and a unit Reynolds number of 4.0×10^6 per foot. A photograph of the model mounted in the NASA-Ames 14-foot tunnel is shown in Figure 1.

The overall test philosophy was to examine the uncontrolled cavity at various Mach numbers and angles of attack to obtain "baseline" conditions and determine what, if any, flow control devices may be required to suppress cavity resonance and optimize the aero-mechanical environment. Next, a series of flow control devices was added to determine their effect on flow quality. Finally, when a small sub-set of aero-mechanically optimal flow control devices was obtained, the aero-optical properties of the shear layer were determined.

III. RESULTS AND DISCUSSION

III.1 Boundary Layer Thickness Establishment

Because of the known sensitivity to boundary layer thickness of the operation of any flow control device in the presence of an on-coming boundary layer, the initial portion of the test was aimed at establishing the correct boundary layer thickness just ahead of the SOFIA aperture. On the full-scale vehicle, the boundary layer thickness provided by the Boeing Commercial Aircraft Company is estimated to be near 8.0 inches. When scaled to the 7% model, this translates to a boundary layer thickness of 0.56 inches. Boundary layer thickness measurements were made with the cavity closed at a station on the model where the upstream edge of the aperture would be if the cavity were open. ("Cavity closed" here signifies the basic aircraft fuselage configuration, not the final "cavity door closed" configuration for the SOFIA aircraft.)

The clean model, that is one void of any artificial boundary layer thickening devices, yielded a boundary layer thickness at the upstream edge of the aperture of only 0.35 inches. Numerous trip devices (denoted as Configurations 3 through 24) were tried on the model nose and just aft of the wind screen until the layer was thickened to an acceptable boundary layer thickness. Boundary layer profiles obtained at the upstream edge of the aperture indicated boundary layer thicknesses of approximately 0.55 inches using trips at the nose and trips stationed just downstream of the wind screen (both 0.030 inches high) over the entire circumference ahead of the cavity in any useful elevation. These trips are very thick by comparison with those normally used for obtaining turbulent boundary layers on relevant lifting aerodynamic surfaces. However, the thick trips were required to produce a correctly scaled boundary layer. Because of the unknown effects

that the large trips may have on details of the turbulent flow over the aperture, these trips were removed in a later portion of the test to ensure the operability of the flow control devices optimized for the thickened boundary layer.

Rakes of pitot probes were mounted on the model to obtain boundary layer information. The local Mach number was determined from these pressures and a nearby surface static pressure. The velocity profiles were obtained from these local Mach numbers and the shear layer static temperatures as determined from the Mach numbers and tunnel total temperatures. Figure 2a shows a summary of the boundary layer profiles obtained at five elevation angles for the representative Mach number of 0.85 and 2.5 degrees angle of attack. These profiles were obtained at the forward station on the model corresponding to the location of the upstream bulkhead. As is evident, the boundary layer is approximately 0.5" to 0.6" thick depending on the definition one might choose for locating the velocity boundary layer edge. Five profiles obtained around the circumference of the body indicate that, with the exception of the profile in the very lowest elevation, all of the profiles are quite similar, and even at the low elevation the profile has about the right kind of thickness. Figure 2b shows the profiles obtained with the closed cavity at the same five elevation angles at Mach 0.85 and 2.5 degrees angle of attack at a downstream station that corresponds to the location of the aft bulkhead. Boundary layer thicknesses at this downstream station correspond to about 0.8". These boundary layer thicknesses, when scaled to the full-scale aircraft, give the required thickness of a little less than 12". Additional boundary layer survey data are given in Reference 3. With the boundary layer thickness properly set, the close out was removed and the open cavity portion of the test was begun.

III.2 Cavity Quieting

III.2.1 Wind Tunnel Results

The initial aperture considered in the present study was one encompassing the entire length from bulkhead to bulkhead and the whole elevation angle ranging from near the crown of the aircraft to a very low elevation. This large rectangular opening is shown in the photograph of Figure 3 and represents a worst-case scenario for attempting to deal with cavity resonance. As expected, in the absence of any flow control devices, this large aperture (Configuration 25) resulted in cavity resonance. This cavity resonance can be depicted with the aid of a power spectral density (PSD) of a representative unsteady cavity pressure transducer as shown in Figure 4. This PSD shows the existence of at least one fundamental frequency and several harmonics present in the range between about 1 Hz and 20 kHz. Figure 4 shows that the cavity, when fully open, resonates, and a quieting control mechanism must be provided either for the full or limited sub-apertures of the cavity to be useful for astronomy purposes. The first cavity quieting attempt was to simply use a porous fence that was a scaled-up version of that which currently operates with success on the KAO. The fence extends circumferentially beyond the aperture in both the upper and lower elevation angles. This fence is 40% porous and its height is 7% of the cavity length measured in the streamwise direction. As can be seen in the photograph of Figure 5, this porous fence (Configuration 28) represents a large perturbation to the aircraft. However, the cavity is successfully quieted, as shown in the PSD of Figure 6, which indicates the elimination of all resonance effects, and has an overall sound pressure level (SPL) of 143 dB (cavity measured) from the remaining random pressure fluctuations in the cavity. These SPL values appear to be quite high; however they apply to the wind tunnel conditions only and (as discussed in the next section) flight values are expected to be about 11 dB lower.

Several other variants of shorter fences and modified porosity distributions of fences were tried in an attempt to reduce the remaining random pressure fluctuation levels with and without aft ramp treatments in place. These studies are detailed in References 4 and 5.

Information such as that shown in Figure 6 was obtained from a single transducer located at one specific location within the cavity. In order to assess the performance of the shear layer control technique at other points in the cavity, other transducers were located on the forward bulkhead and the aft bulkhead in various positions. How well the flow control device performs throughout the cavity can be depicted in figures similar to that given in Figure 7. This figure shows the overall sound pressure level (the integral over all frequencies of the PSD) at several sites in the cavity with the 7% porous fence and the full aperture opening at a Mach number of 0.85 and seven different angles of attack. The horizontal scale indicates different pressure transducer locations on the cavity bulkheads; e.g., ULA is the upper left transducer on the aft bulkhead and LCF is the lower center transducer on the forward bulkhead. Other Mach numbers were tested and were shown to all be free of resonance. This finding is consistent with previous experience that has indicated a wide operating margin for porous fences. As can be seen in Figure 7, the SPL is approximately the same for all the locations within the cavity. This situation is in contrast to that known to exist on the KAO, where pressure fluctuations vary substantially in the cavity from near the fuselage (top of cavity) to the floor (bottom of cavity). This is most likely due to the ineffective flow control produced by the porous fence on that configuration.

Because of the suspected additional optical degradation caused by a porous fence and its high inherent drag, techniques involving the use of no forward treatment were investigated. One involved the use of an aft ramp on the full-open aperture as shown in the photograph of Figure 8. For this configuration (30), resonance is still present as shown in Figure 9, even though the overall SPL is only 142.5 dB at α = 2.5 degrees. Figure 10 shows that this configuration has no margin for lower angles of attack, thus other configurations were investigated. Most of these (Configurations 31 through 48) were only partially successful at controlling resonance and producing a low SPL value over the Mach number and angle of attack ranges. Details are given in Reference 4.

Since the size of the open aperture required at any time during astronomy observations is only dictated by the diameter of the primary mirror and telescope excursions associated with elevation and cross elevation motions to maintain tracking, plus the tracker and acquisition camera apertures, it was decided to attempt to limit the aperture while maintaining the same cavity volume as discussed previously. The first limited aperture tested and discussed here is known as the "limited aperture high" position (Configuration 50). This position is the nominal 60 degree observation elevation angle. Limitations on aperture size were constructed by putting in place various close outs over the lower and uppermost portions of the full aperture. A photograph of the high position is shown in Figure 11. An aft ramp was in place for this configuration and no upstream treatment was used. This configuration resulted in one of the quietest cavities that had ever been obtained in the 14-ft wind tunnel. A representative PSD is

shown in Figure 12 for Configuration 50. The overall SPL for this configuration at M = 0.85, α = 2.5 degrees was 137.3 dB. With the success obtained at the uppermost elevation angle, limited apertures were constructed for the mid and low elevations. The success obtained at the high angles was not found for these lower angles. Much higher random pressure fluctuations were found at the mid elevation, while at the low elevation angle the cavity exhibited a resonance structure similar to that for the full open aperture.

In an attempt to control the cavity resonance at the limited aperture low position, a large series of tests was conducted using various moldings made up in real time during the test. These moldings were attempted as a result of surface oil flow studies that indicated large flow variations exist near the apertures in both of the lower elevation positions. Large flow angularity and the unknown effects of the pressure gradients that exist over the open cavity were suspected of causing the cavity resonance. In order to better accommodate the high flow angularity, moldings were made that smoothly blended the aft ramp contour into the downstream corners of the previously rectangular limited aperture. The aft ramp used here was a 30 degree ramp with a full-scale length (forward of the aft bulkhead) of 40 inches. Success was obtained in cavity resonance elimination using this feature for the limited aperture low elevation condition. To further control cavity resonance in an attempt to produce the best optical performance, semi-circular close outs were developed for use on the upstream two corners of the aperture. This led to a quasi-elliptical aperture that proved to be successful in eliminating cavity resonance and producing a very low overall background pressure fluctuation level. A photograph of this treatment (Configuration 98) is shown in Figure 13. A PSD of the pressure fluctuations obtained with this configuration is shown in Figure 14. The SPL

for this configuration 137.2 dB. Intermediate configurations leading to this final configuration are discussed and the data presented in References 4 and 5.

Once the cavity resonance and flow control issues were resolved at the low elevation, the configuration was changed to the limited aperture mid elevation position and, again, moldings were constructed that were conformal with the fuselage aperture and aft ramp at this elevation angle. These moldings are slightly different in shape than those developed for the low elevation configuration because of differences in the mold line of fuselage at these locations. A photograph of this mid elevation configuration is shown in Figure 15 and the PSD is shown in Figure 16. The SPL is 135.6 dB.

To complete the sequence, molded aft and semi-circular close outs were developed for the limited aperture high elevation angle (Configuration 101) and were applied. A photograph of this configuration is shown in Figure 17 and the PSD is shown in Figure 18. The resulting SPL is 135.9 dB. Configurations 98, 100 and 101 were tested later with the probe drive in place of the telescope model. When the probe drive was in place, these configurations are numbered 109, 111 and 106 respectively.

These molded configurations represent the best cavity quieting treatments with the least disturbance to the flow field. Because they use no upstream treatment, it would be expected that their aero-optical performance will be better than treatments such as a fence and this is discussed in a later section of this report. Good operating margin with Mach number, angle of attack and yaw angle is demonstrated by these configurations. In the limited aperture low arrangement, a scaled 6" forward facing step

located on the aft portion of the ramp (Configuration 99) was tested and showed no loss of performance. The SPL for these three configurations is about the same so that a smooth transition from one elevation angle to another is expected. The limited aperture elevations tested here correspond to 14, 40 and 64 degrees for the low, mid and high positions, respectively.

The next three configurations mentioned here are the result of the desire to develop comparable information for use in decisions in the aero-optical portion of the test. The limited aperture configurations were tested with a porous fence for the high, mid and low limited apertures which had the probe drive in place (and not the telescope model) and were numbered Configurations 110, 112, and 104. Configuration 103, with the telescope model in place, was the same treatment as Configuration 104. These configurations are discussed extensively in the aero-optics portion of this report as baseline data to be compared with the molding quieted cavities. Power spectral densities from these limited aperture configurations do not show a substantial improvement over those obtained with the fence ahead of the fully open aperture, thus indicating a fundamental limitation of the fence as an anti-resonance and cavity quieting device.

In addition to the behavior of the pressure variation field within the cavity, pressure variations downstream of the aperture and on the fuselage are of interest since any anti-resonance device may cause unsteady variations in the pressure field to exist where none have been prior to modifying the fuselage flow field. A measure of the performance of the various cavity quieting techniques can be discussed through the aid of Figure 19, which shows the overall sound pressure level upstream, over and

downstream of the open aperture on the fuselage. There are no data where the cavity is located (between model stations 36.4 and 49.0). Three configurations are compared for a line of instrumentation through the low elevation position. The porous fence (103) produces an average SPL that is higher than even the resonating cavity (25), while the molded configuration (98) produces very low level fluctuations. The fence produces larger pressure fluctuations within the cavity and these larger variations are also felt downstream. On the other hand, the molded configurations produce pressure fluctuation levels that are as quiet as, if not quieter than, those observed in the absence of an open aperture. This is a very significant finding, since much effort and cost has been required in past airborne open cavity installations to minimize the effect of pressure fluctuations downstream of the aperture. These lower values could significantly extend the fatigue lifetime of the vehicle's structural components downstream of the open aperture.

III.2.2 Scaling Cavity Pressure Fluctuations to Flight

Pressure fluctuations are known to scale with freestream dynamic pressure. This scaling has been established through many years of wind tunnel and flight testing (e.g., Reference 6), and is a useful parameter when considering wind tunnel and/or flight data which have not been taken at the same conditions. Since the dynamic pressure scales as the square of the flight Mach number and linearly with the external pressure, one can immediately translate the wind tunnel data to the flight condition. The dynamic pressure used in the wind tunnel is approximately 3.5 times that encountered on the SOFIA at operating altitude. This produces a decrease of approximately 11 dB. When applied to the molded configurations with an average 136 dB value in the wind tunnel, the flight values become about 125 dB. These values can be expected to exist

everywhere in the cavity on the SOFIA. This is in contrast to the observed behavior of the pressure fluctuation levels on the KAO with the porous fence in place. Previous experiments have shown that a value of 125 dB can be obtained only near the bottom of the KAO cavity while the pressure fluctuations near the top of the cavity range up to 20 dB higher than that value. This is because there is a contribution to the overall sound pressure level near the upper part of the cavity associated with the poor shear layer control that exists on the KAO. Other SOFIA cavity pressure fluctuation levels obtained in the wind tunnel can be scaled to flight by subtracting 11 dB from the tunnel values. Based on the current wind tunnel results and known scaling relationships, it can be concluded that anti-resonance configurations similar in performance to the molded control devices discussed here can produce an environment as benign as any airborne platform operating today.

The aero-mechanical issues are a major concern for any airborne open-cavity installation. However, what must next be considered are the optical effects of the demonstrated resonance suppression techniques. The following section discusses these aero-optical considerations.

III.3 Aero-Optical Issues

III.3.1 General Considerations

Several wind tunnel tests have been conducted in the past considering the optical implications of the aerodynamic flow fields derived from various flow control devices. Aerodynamic information is obtained from both steady-state and unsteady-state measurement systems. A procedure (References 2 and 7) used here relates the statistics

of the unsteady aerodynamic field to aerodynamically inferred optical wavefront errors, and these wavefront errors can be used to estimate the optical performance of various detector systems located within the open cavities controlled by the various shear layer control techniques.

This procedure has been validated recently (Reference 2) and is briefly outlined here. In that study, portions of the current experiment were examined in light of previously obtained aerodynamic data on the KAO at full-scale and in flight at astronomy operating altitude. Turbulent scales sizes, total shear layer width and optical wavefront errors scaled from the 14-ft wind tunnel test at a 10% scale of the KAO were shown to be effectively reproduced when compared with the full scale flight data. This comparison validates the approach taken in the present study of measuring aerodynamic flow fields that affect optical performance and scaling these results to flight. This section discusses representative flow conditions and aerodynamic data obtained for deriving the expected optical distortions associated with each of the configurations at various positions in the aperture at three elevation angles.

To determine the optical losses associated with the shear layer over the top of the open cavity, either direct optical measurements or inferences from aerodynamic measurements must be made. The latter approach is used here. Equation 1 relates the optical wavefront variance to an integral along the beam path of the square of the density fluctuations times the integral scale lengths of those fluctuations and the Gladstone-Dale constant:

$$\sigma^2 \equiv 2\beta^2 \int_0^L \overline{\rho'^2(r)}\ \ell_r\, dr \qquad (1)$$

where β is the Gladstone-Dale constant, ρ is the density fluctuation and ℓ_r is density fluctuation scale size in the r (viewing) direction.

Equation 1 requires the independent determination of the magnitude of the density fluctuations and their integral scale sizes. Magnitudes of the density fluctuations can be deduced as set forth in Reference 1 by measuring the unsteady mass flux fluctuations and relating the density fluctuations to those mass flux fluctuations through the mean Mach number within the shear layer at each point. Thus, in addition to the obvious parameters from Equation 1, the mean Mach number profile must be obtained. In the present study, the mean Mach number profiles were obtained from pitot pressure surveys through the shear layer, combined with the cavity static pressure to infer the local Mach number. This procedure was validated in the present test by direct measurements of the static pressure within the shear layer and beyond its edge into the remaining flow field.

III.3.2 Mean Shear Layer Profiles

The mean Mach number profiles were obtained for several configurations and at several locations within the aperture of each configuration. The center of the

aperture is denoted by the coordinate x = 0, y = 0, where x is the streamwise distance and y is the elevation distance measured positive towards the higher elevation angle. Only cases for which cavity resonance has been suppressed were surveyed to obtain aero-optical data. Two primary anti-resonance treatments were used during this portion of the study. The first is a reference case which is the tall fence configuration at each of the three elevations (Configurations 110, 112 and 104). The second case is the molded configuration at each of the three elevations (Configurations 101, 100 and 98). These configuration numbers apply to the aero-mechanical portion of the test with the telescope model in place. When the probe drive was used with the molded configurations, these same configurations became 109, 111 and 106 respectively from high to low elevation limited aperture position.

The local Mach number varies from near zero in the cavity to its maximum value at the outer edge of the shear layer. Mean profiles of the Mach number were obtained at numerous locations in the aperture for the three elevation angles for the two representative classes of flow control.

An example of the variation of these mean profiles is shown for the molded configuration at the mid elevation position (111) in Figure 20. The mean Mach number profiles are plotted as a function of distance (z) away from the nominal mold line of the aircraft at the location at which the survey is made. The pitot tube arrangement used for making these Mach number surveys contained an upper and a lower tube, and where these measurements overlap they indicate the repeatability and the stability of these shear layers over the molded configuration. These profiles were taken for the representative

condition of M = 0.85, α = 2.5 degrees, as are all of the remainder of the aero-optical data considered in this study. Figure 20 demonstrates the evolution of the initially thin shear layer evolving from the upstream fuselage boundary layer. The shear layer width increases with increasing streamwise distance while the mean gradients in the layer decrease. This result represents a very detailed survey taken at several streamwise positions in the aperture. These profiles were taken at the mid elevation angle at the center, that is y = 0 position. The mean Mach number profiles are useful for understanding the evolution of the shear layer and may be used to establish the behavior of the upper limit of integration in Equation 1. This upper limit is just the total shear layer width determined from the mean profiles. The behavior of this width for the fence and molded configurations as a function of streamwise distance is shown in Figure 21. This thickness parameter is determined without regard to where the actual shear layer is located, but only examines its total thickness. As can be seen in Figure 21, there is a general trend of all the data that represents an increase in the shear layer width with streamwise distance. The streamwise distance is assumed to be zero at the center of the aperture, negative in the upstream direction and positive downstream. There are variations that occur in the value of the parameter that are well beyond the uncertainty (about 10% of the local value) in determining these values. For example, near the center of the aperture for the mid elevation, the thickness of the fence shear layer is much larger than that of the molded configuration. On the other hand, the comparison between these two configurations in the upstream and downstream portions of the aperture is reversed. When considered as a whole, the differences between the fence and molded configurations are small. It will be shown later that there is a large optical difference in these configurations, but it is not simply related to differences in the total

shear layer width. Selected mean profile information obtained during the present study is shown in Appendix I and additional profiles are given in References 8 and 9.

III.3.3 Integral Scale Length Considerations

The integral scale length is determined by cross correlating a pair of sensors from a rake that was positioned at various locations throughout the shear layer. Figure 22 shows a photograph of this rake installed on the model. The spatial correlation function which yields the integral length scale required in Equation 1 is obtained from the time correlation functions between several pairs of sensors in the shear layer. This process is shown schematically in Figure 23, which depicts time-correlation functions for three pairs of sensors located at a distance in the shear layer of z = 0.1". This information is for a representative configuration. As can be seen, the time auto correlation function at zero time delay has a value that decreases as the probe separation increases. A plot of this correlation value versus sensor separation distance is depicted in the lower portion of the figure. The curve has the equation shown on the figure and indicates that the integral scale length is 0.24". This process is repeated at several points throughout the shear layer at each measurement position in the aperture.

Figures 24 and 25 show representative distributions of integral scale length throughout the shear layer near the center of the aperture for the two configurations of interest here. Figure 24 shows the scale lengths for the fence in place, while Figure 25 shows the distribution for a molded configuration. The maximum scale lengths occur for the fence case for this representative condition at the center (x = 0, y = 0) of the mid elevation aperture.

It is clear from the representative data shown in Figures 24 and 25 that the integral scale sizes differ, at least at the center position between the fence and the molded configurations. Similar data may be used to examine the variation of scale sizes in the streamwise direction. Of particular interest is the ratio of the scale size to the total shear layer width. The shear layer width has been previously shown to be relatively constant for each of the configurations being discussed here. The values for the ratio of scale size to shear layer width are shown in Figure 26. It is clear that there is a substantial difference between the fence and molded configurations. The fence configuration indicates that the scale size is approximately 20% of the shear layer width and it is essentially independent of streamwise position. On the other hand, the moldings indicate that initially the ratio is near a value of 0.1. This is the value known to exist in an equilibrium, attached turbulent boundary layer and this 10% value would be expected to be present at the upstream edge of the aperture. The relatively long transition between this boundary layer-like ratio and the final data obtained in the downstream portion of the aperture is of interest since the smaller this ratio is the better the aero-optical performance will be. Figure 26 defines a fundamental difference between the porous fence and the molded configuration. Another one, of aero-optical importance, is the difference in the density fluctuation levels.

To fully use Equation 1 to determine the optical phase distortions, these scale lengths must be supplemented with the amplitudes of the fluctuating density. The following section discusses the determination of the fluctuating density and the use of Equation 1. The remainder of the length scale data obtained in the present study is presented in Appendix II.

III.3.4 Aerodynamically Inferred Optical Phase Variance

Density fluctuation information is derived from the recorded electrical signals proportional to the mass flux fluctuation. The data are reduced to distributions of rms fluctuating density as a function of position throughout the shear layer using the technique presented in Reference 1. Figures 27 and 28 show representative distributions of rms density fluctuation through the two shear layers corresponding to the positions discussed in Figures 24 and 25. Peak fluctuation values for the fence are higher than those for the molded configuration. This difference arises because the scale sizes (that drive the fluctuation levels) are fundamentally different for these two configurations, as noted previously. The remainder of the density fluctuation data obtained in the present study are presented in Appendix III.

The density fluctuation values of Figures 27 and 28 must be squared and multiplied times the scale length to obtain the integrand of Equation 1. Plots of these integrands are shown in Figures 29 and 30 for the fence and molded configurations at the center of the mid elevation aperture. Again, both the scale sizes and density fluctuation levels are higher for the fence configuration; however, because of the squaring of the density fluctuations, their contribution to the increase of the integrand is the main cause of the increased distortion for the fence. From these two plots, one can see that the integral of these curves will be quite different, with the phase variance for the moldings being much lower than the fence. The remainder of the integrand data obtained in the present study is presented in Appendix IV.

Information concerning the mean fluid density, the fluctuating rms density, the scale sizes and the integrand for Equation 1 are summarized for the representative fence and molding cases in Figures 31 and 32. These figures also contain the integrated, aerodynamically deduced wavefront error at the bottom of each figure. For the configuration with the fence, the expected wavefront error (the square root of the phase variance) at the center of the mid elevation in the wind tunnel is 0.059 microns, whereas for the case with the moldings, the wavefront error is only 0.035 microns. If an average wavelength of 0.53 microns is used, the σ/λ errors are 0.112 and 0.065 waves respectively for the fence and moldings. Again, these are representative measurements located near the center of the aperture and the wavefront errors discussed here apply to the wind tunnel conditions only. How these wind tunnel σ/λ values vary over the aperture for the high, low and mid elevation angles is depicted in Figure 33. The remainder of the summary data obtained in the present study is presented in Appendix V. In order to assess expected wavefront errors on the full-scale aircraft, known scaling relationships must be applied.

III.3.5 Scaling Aero-Optical Phase Errors

In general, it is difficult to scale the optical performance of a given anti-resonance system since scaling laws for optical performance, per se, are not well understood. However, the wavefront error produced by a given shear layer is scaleable to other flight environments through the use of known aerodynamic scaling relationships and knowledge of how the resulting aerodynamic flows affect optical performance. Since Equation 1 contains two geometrical terms, the scale length and shear layer width, and one characteristic of the fluctuating density, the scaling is relatively straightforward. The

aircraft Mach number can influence the magnitude of the density fluctuations and, as shown in Reference 1, the rms density fluctuations are proportional to the square of the flight Mach number. The magnitude of the fluctuating density scales simply with mean density. The mean wind tunnel density is substantially higher than the atmospheric density at the operating altitudes, and, in fact, $\rho_{flight}/\rho_{tunnel}$ has a value of about 0.36 for a 43,000 foot operating altitude. On the other hand, both the scale size and shear layer width are known to scale linearly with the scale size of the test article (Reference 7). The model scale is 0.07, so that scale sizes and shear layer widths can be expected to be 14.3 times larger on the SOFIA than they are in the wind tunnel. Slight changes in these sizes due to differences in wind-tunnel and full-scale flight Reynolds number are negligible for purposes of the present discussion. When considering the geometric and mean density scaling, the overall scale factor has a value for $\sigma_{flight}/\sigma_{tunnel}$ of 5.14. Thus the wavefront errors discussed in the previous section must be multiplied by this scaling factor to be consistent with those expected at operating altitudes for the SOFIA.

Variations over the aperture of the scaled wavefront errors are shown for the full-scale SOFIA in Figure 34. The molded configuration has a σ value less than $\lambda/4$ in the forward half of the aperture, indicating excellent optical performance, while the wavefront errors from the fence (and downstream molding values) have values up to nearly a full wave. Values of σ/λ less than 0.25 are very important since the Strehl ratios resulting from these wavefront errors are about 0.1 or larger. This high value indicates that negligible image resolution would be lost in the visible due to the shear layer in the forward portion of the aperture. For observations at other wavelengths, these data can be used to estimate the focal plane behavior.

III.3.6 Focal Plane Behavior

Information such as that presented in Figure 34 can be used in conjunction with further aero-optical analyses to define the nature of the image at the focal plane of an imaging system. In a recent report (Reference 10), a simplified equation was presented that allows the combined effects of diffraction and turbulent flow to be determined. Equation 15 from Reference 10 was used to compute the effects of the variation of focal plane spot size with wavelength for two cases of interest here. This equation allows the combined effects of diffraction and turbulence to be calculated over an entire aperture where the wavefront error is assumed to remain constant). Since, as is evident from Figure 34, this is not the case, the following discussion is only an approximation to the type of behavior that might be expected. This approximation is used here specifically to show the differences between the molding- and fence-quieted cavities. Again, the limited aperture, mid elevation condition is chosen.

Results of the point spread function calculations have been integrated here to determine the encircled energy diameter containing 84% of the total energy at the focal plane. The wavefront errors and scale sizes required for this calculation were taken from near the center of the aperture. The results of this calculation for blur circle diameter are shown in Figure 35. The asymptotic slope beyond wavelengths larger than 10 microns is the diffraction limit. For shorter wavelengths, increases in blur circle diameter due to turbulence effects are evident. The very short wavelength limit of approximately 17 micro-radians, or a little less than 3.5 arc seconds, is also evident. For the molding configuration, the turbulence effects have diminished substantially for wavelengths beyond

about 4 microns. On the other hand, for the fence quieted configuration, turbulence effects are evident out to 7 to 8 microns. Of particular note are the large decreases in spot size evident at about 2.5 microns and 3.5 microns respectively for the molding and fence quieted configurations. Figure 35 demonstrates the significant improvement in aero-optical performance obtained with the molding configurations over that of the fence.

IV. CONCLUDING REMARKS

A wind tunnel test of a 7% scale model of the Boeing 747-SP forebody has been conducted to examine the aero-mechanical and aero-optical effects of a large open cavity designed to accommodate a 2.5 meter telescope. The significant finding of the wind tunnel test is that the cavity resonance can be successfully quieted. Treatments allow a very low residual random pressure fluctuation field to exist within the telescope environment. Two of the successful quieting techniques (a porous fence/aft ramp configuration and a "molding" with an integral aft ramp configuration) were examined here in detail to demonstrate the aero-mechanical performance in the wind tunnel. This information was scaled to a full-scale flight article, and current estimates are that the SOFIA cavity can operate with an overall random pressure fluctuation level in the cavity as low as approximately 125 dB with the idealized molding configuration. Fences, on the other hand, do prevent resonance, but the remaining background fluctuation level is 4 to 5 dB higher than that with the molding configurations.

The same two quieting techniques were also examined here to investigate their aero-optical performance. Shear layer properties over the open cavity were investigated with aerodynamic instrumentation in order to determine their optical performance. Again, the comparison between the molding and fence anti-resonance treatments indicates that the shear layer properties can be made to have a minimal effect on seeing with the use of the moldings and aft ramp.

The moldings used in the present study are very successful and represent a general class of treatment that is likely to produce desireable aero-mechanical and aero-optical

results on the full-scale vehicle. Specific shapes developed here are not unique; however, perturbations away from these shapes were not attempted.

During the course of the present investigation, 119 configurations were tested. Approximately 15 of these duplicated configurations tested previously with respect to the anti-resonance devices, but contained the probe drive rather than the telescope model. Some 24 configurations at the beginning of the test used a closed cavity to establish the correct boundary layer thickness. This analysis report presented the highlights of some of those configurations. Other information not discussed in detail either appears in the Monthly Progress Reports (References 3 through 5) or is contained in the Appendices of this report. In addition to the fence and molding configurations discussed in detail here, louvered configurations devised by Boeing personnel were tested and data for these configurations are presented in the Appendices and a separate Boeing report.

With the successful anti-resonance and excellent aero-optical performance demonstrated by the molding configurations, the risk to proceeding with the design of the full-scale SOFIA aircraft has been substantially reduced. Recommendations for further study appear in the following section.

V. RECOMMENDATIONS

Wind tunnel test findings must be integrated with the on going SOFIA design effort. Implementation of some form of the anti-resonance treatments denoted as "moldings" in this study should be pursued. Practical vehicle design issues must be addressed. The issue of functional cavity door design must be combined with the findings of this study. Additional wind tunnel testing of the concepts devised here and resulting from further design studies is required to ensure their usefulness in the flight/astronomy environment. Specifically, investigations of the sensitivity of aero-mechanical and aero-optical performance of the SOFIA shear layer to practical variations in the demonstrated molding concept (e.g., size and shape changes) should be conducted to assist in development of practical and reliable door designs. Additional analytical work on aero-optical performance of the measured shear layer properties should be conducted to determine the effect of the variation of shear layer properties around the opening on total optical performance.

VI. REFERENCES

1. Rose, W.C. and Cooley, J.M.: "Analysis of The Aerodynamic Data from the AOA Wind Tunnel Test and Implications for the AOA Platform." Final Report Contract DAAH01-85-C-0312, 29 October 1985.

2. Rose, W.C. and Cooley, J.M.: "Innovative Shear Layer Control Methods for Large-Scale Airborne Telescopes." Final Report, Phase I. Prepared for NASA-Ames Research Center under contract NAS2-13034, 31 August 1990.

3. Monthly Progress Report for March on SOFIA Wind Tunnel Test prepared for Sverdrup Technology, Inc., NASA-Ames, 31 March 1990.

4. Monthly Progress Report for April on SOFIA Wind Tunnel Test prepared for Sverdrup Technology, Inc., NASA-Ames, 30 April 1990.

5. Monthly Progress Report for May on SOFIA Wind Tunnel Test prepared for Sverdrup Technology, Inc., NASA-Ames, 31 May 1990.

6. Buell, D.A.: "Airloads Near the Open Port of a One-Meter Airborne Telescope." AIAA Paper 75-71, presented at the 13th Aerospace Sciences Meeting, 28 January 1975.

7. Rose, W.C.: "Aerodynamics of Seeing on Large Transport Aircraft - Progress Report 1 Dec 1985 - 31 May 1986." Prepared for NASA-Ames Research Center under Contract NCC2-382.

8. Monthly Progress Report for June on SOFIA Wind Tunnel Test prepared for Sverdrup Technology, Inc., NASA-Ames, 30 June 1990.

9. Monthly Progress Report for July on SOFIA Wind Tunnel Test prepared for Sverdrup Technology, Inc., NASA-Ames, 31 July 1990.

10. Banish, M.R., Clark, R.L., Kathman, A.: "Wavelength Dependence of Blur Circle Size Through Turbulent Flow," SPIE 1990 International Symposium on Optical & Optoelectronic Applied Science and Engineering; Window and Dome Technologies and Materials II Conference, July 1990, San Diego, CA.

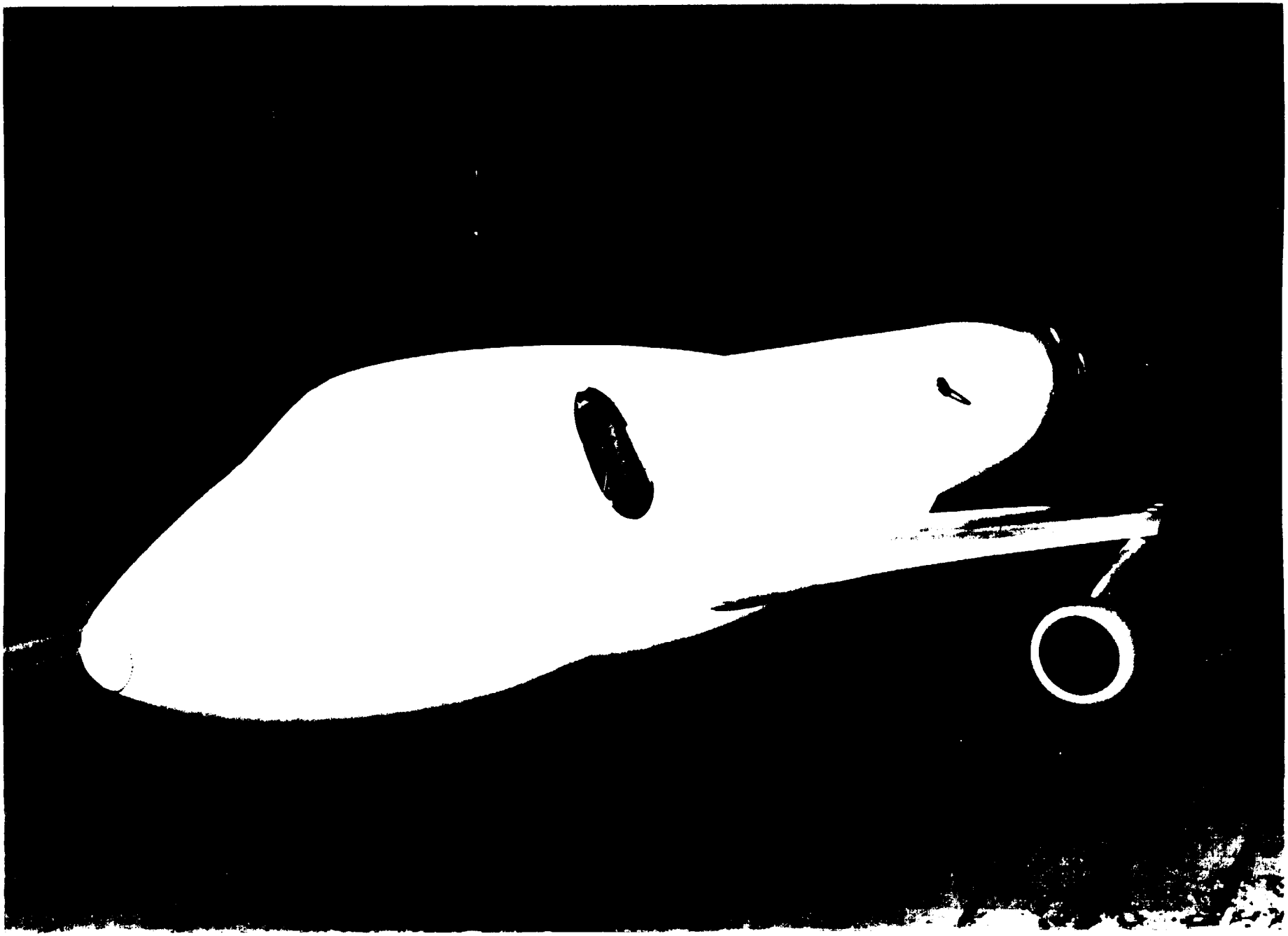

FIGURE 1. Photograph of the SOFIA model mounted in the NASA-Ames 14-foot wind tunnel.

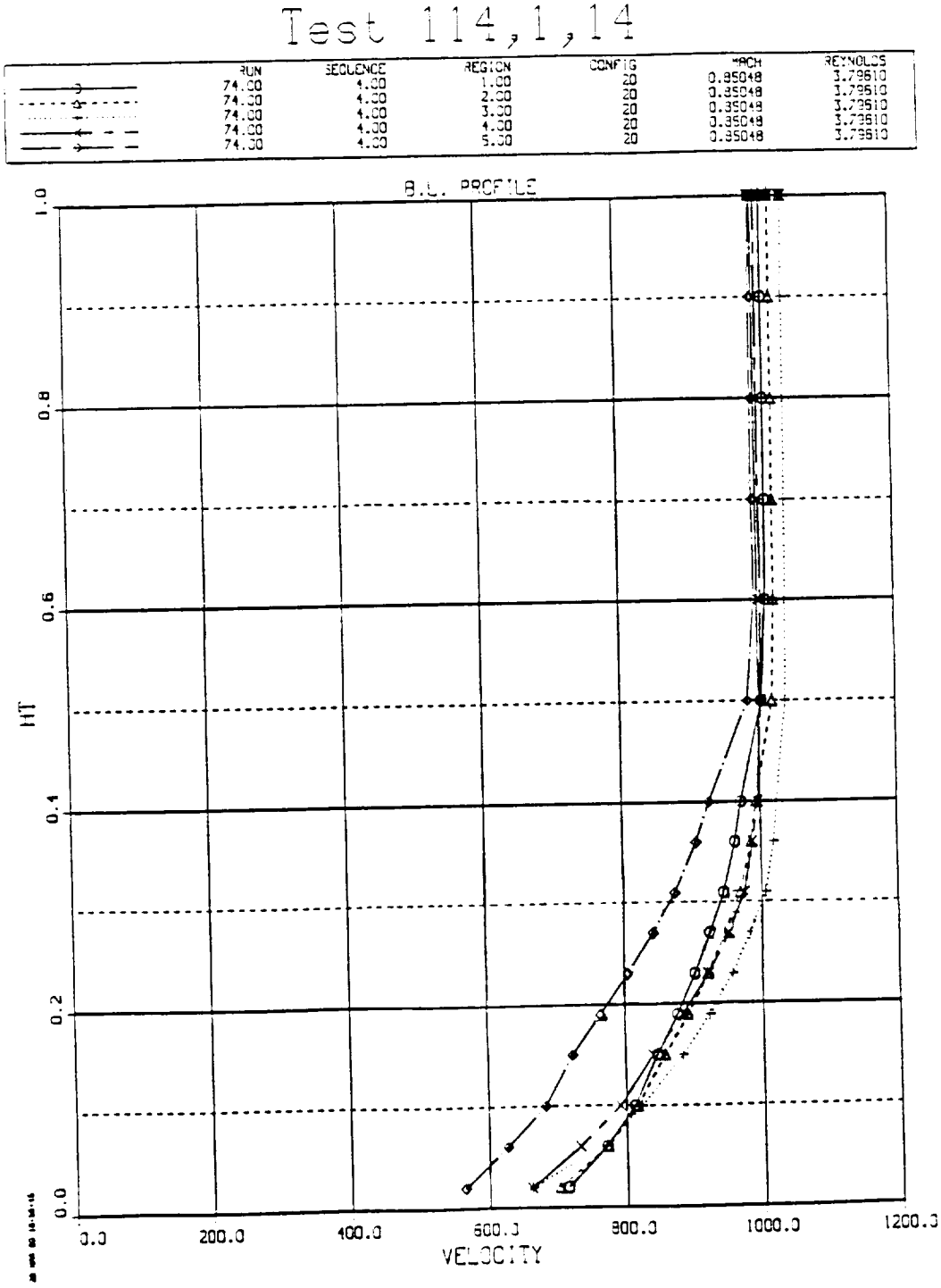

FIGURE 2. Summary of boundary layer profiles at five elevation angles at M = 0.85 and α = 2.5 degrees.

(a) Forward station.

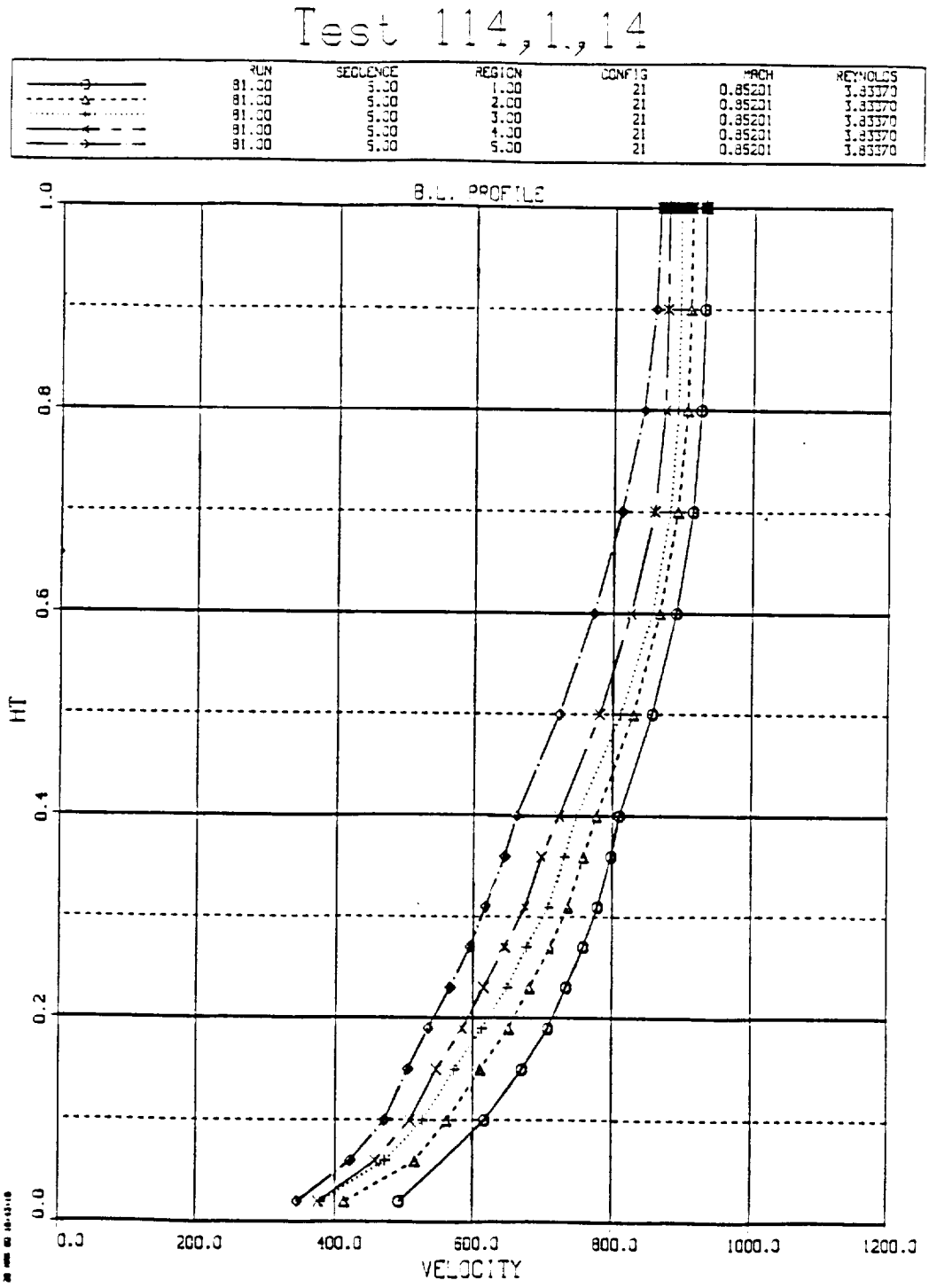

FIGURE 2. **Concluded.**

(b) Aft station.

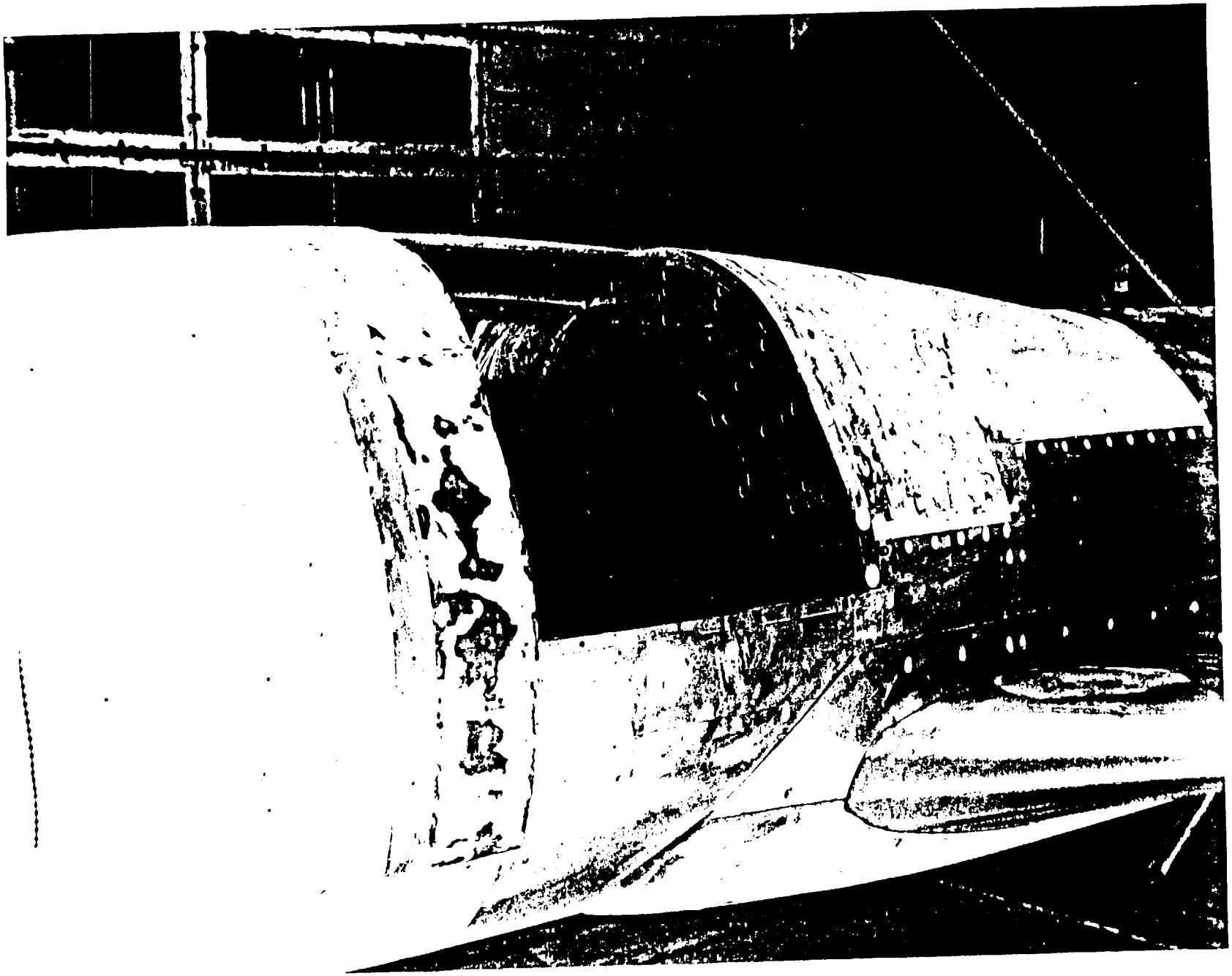

FIGURE 3. Photograph of the SOFIA model with the full aperture, untreated open cavity (Configuration 25).

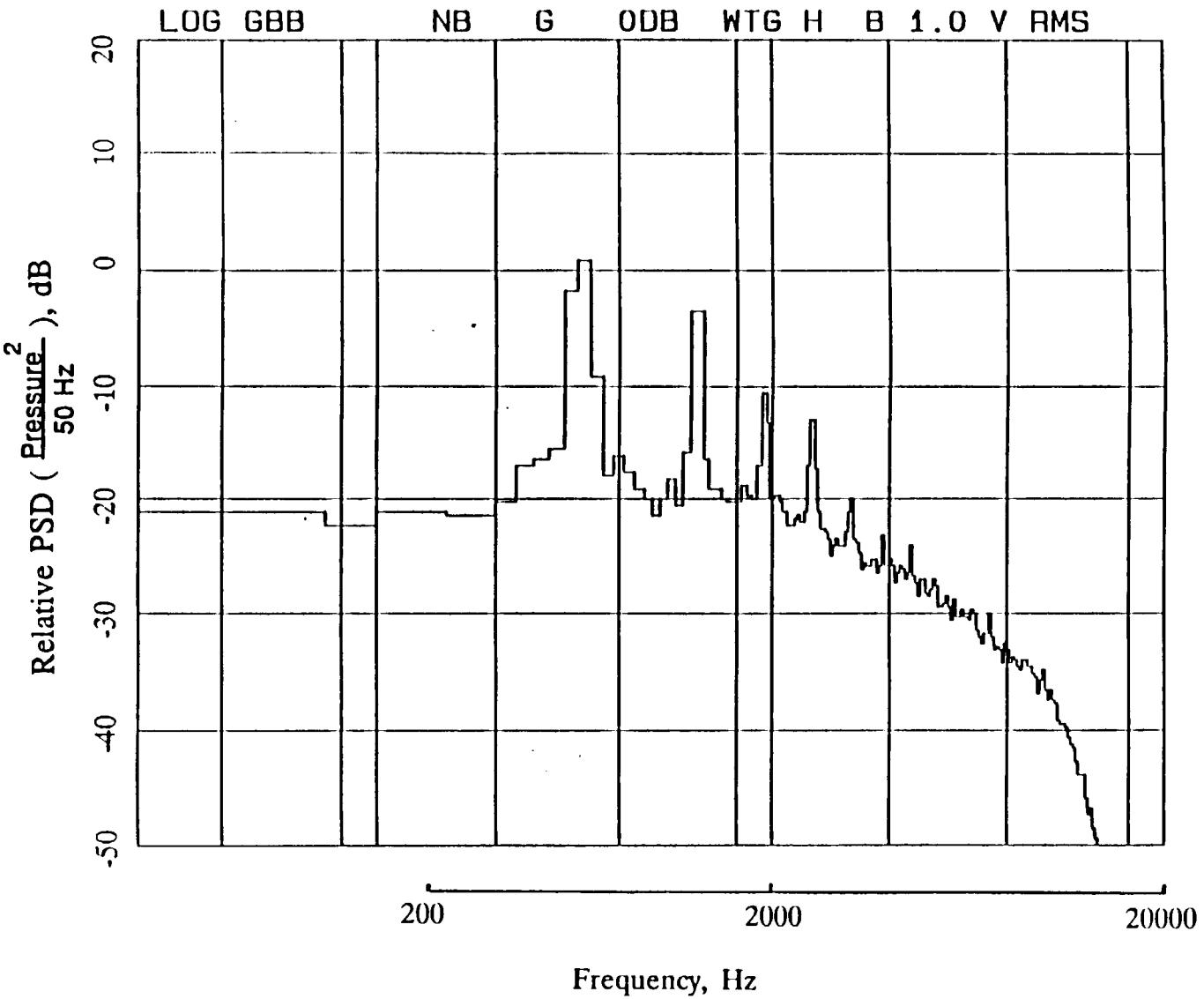

FIGURE 4. **Pressure fluctuation spectrum for Configuration 25 (resonating cavity) at M = 0.85 and α = 2.5 degrees.**

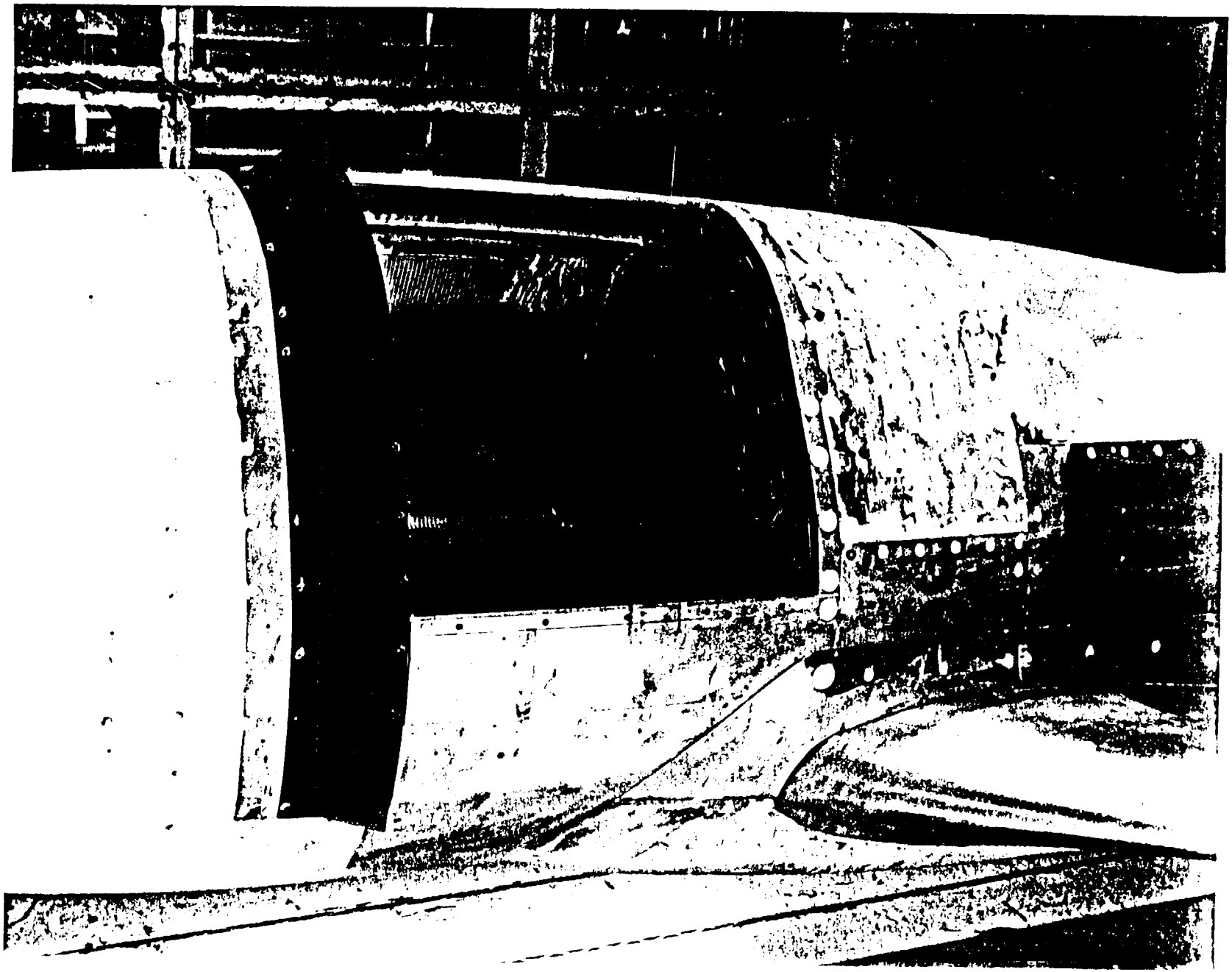

FIGURE 5. Photograph of the SOFIA model open cavity with a 7% high, 30 degree, 40% porous fence (Configuration 28).

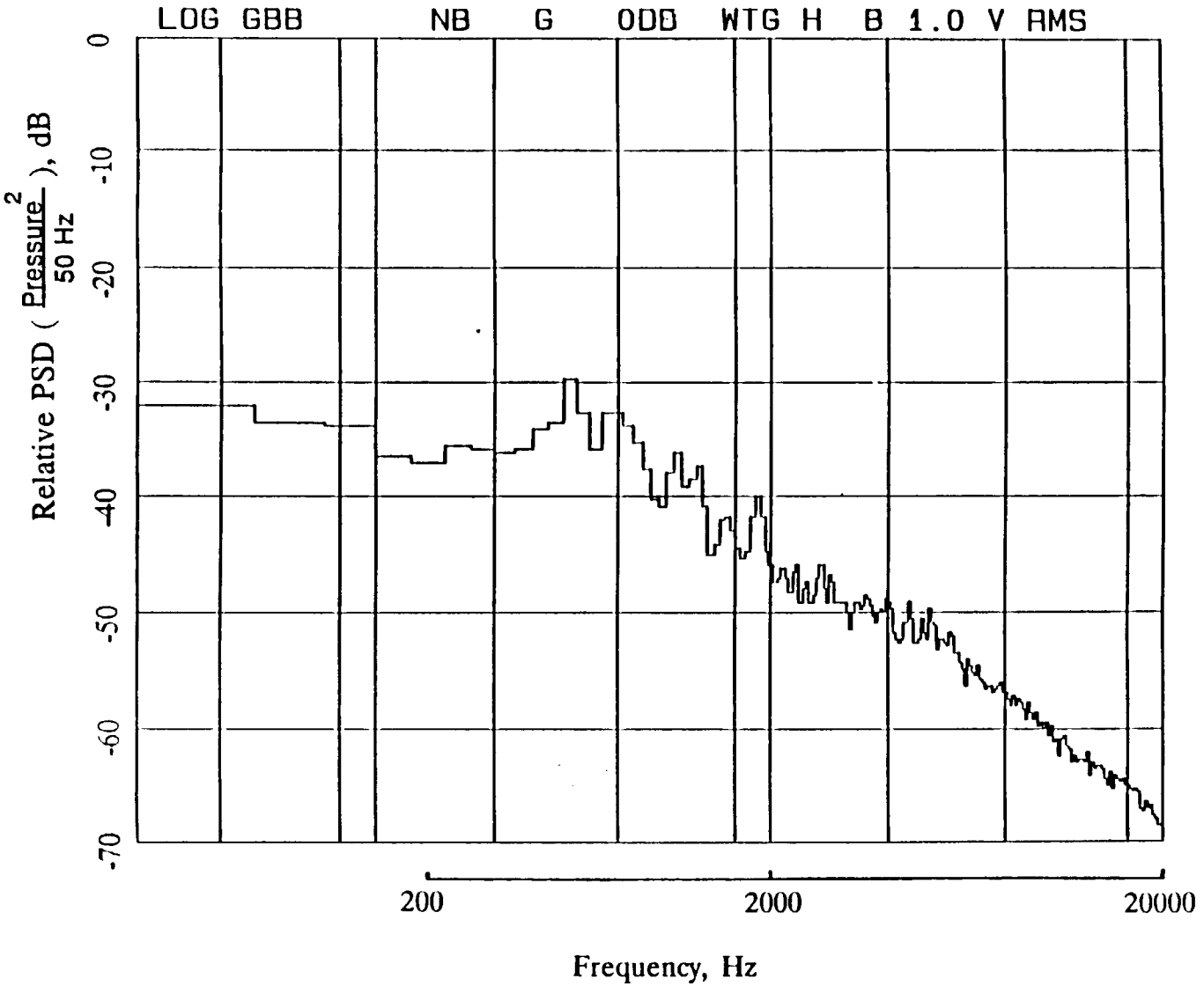

FIGURE 6. **Pressure fluctuation spectrum for the full aperture, fence quieted cavity (Configuration 28) at M = 0.85 and α = 2.5 degrees.**

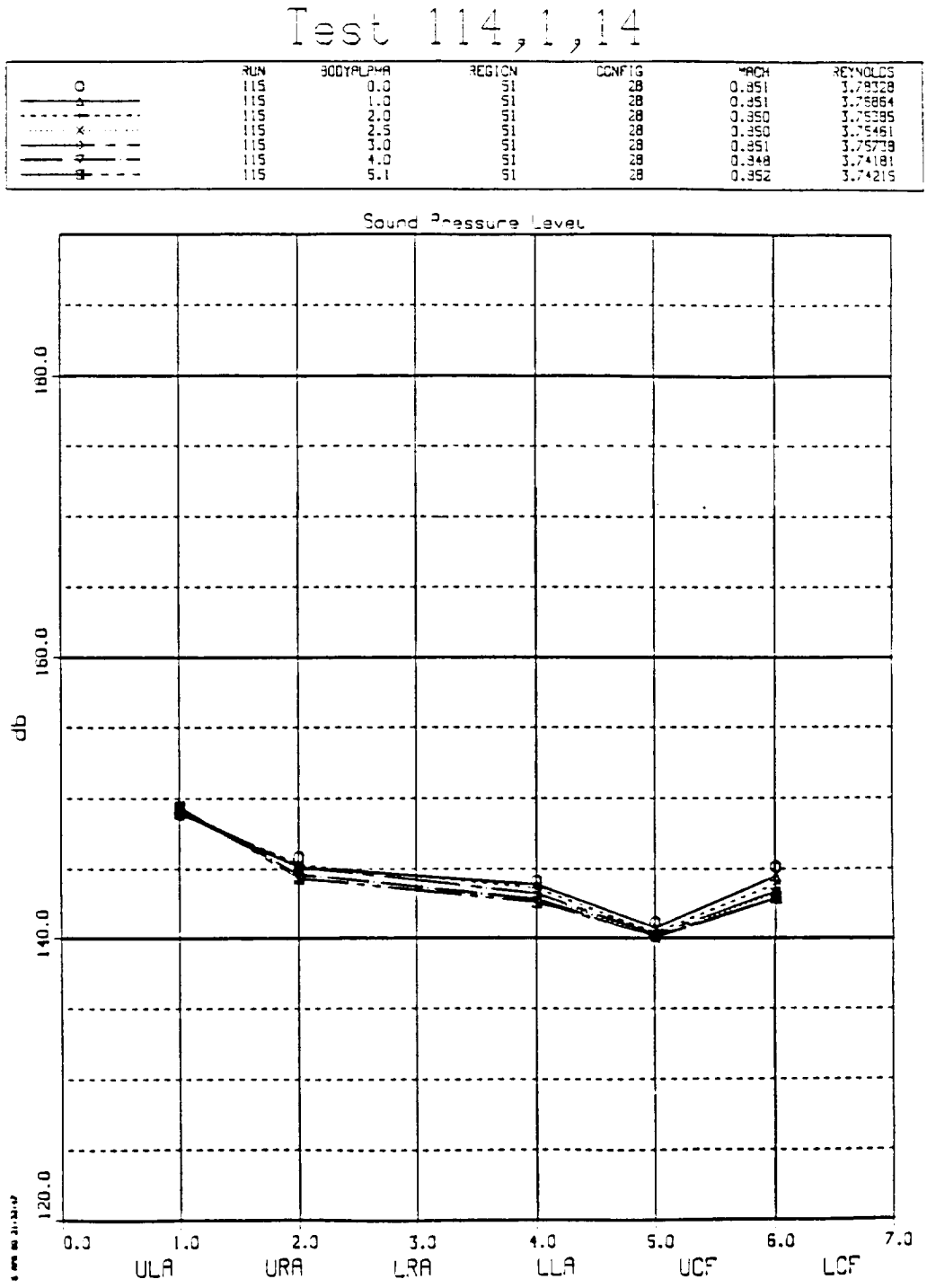

FIGURE 7. **Sound pressure level comparisons for the full aperture, fence quieted cavity (Configuration 28) at various angles of attack for M = 0.85.**

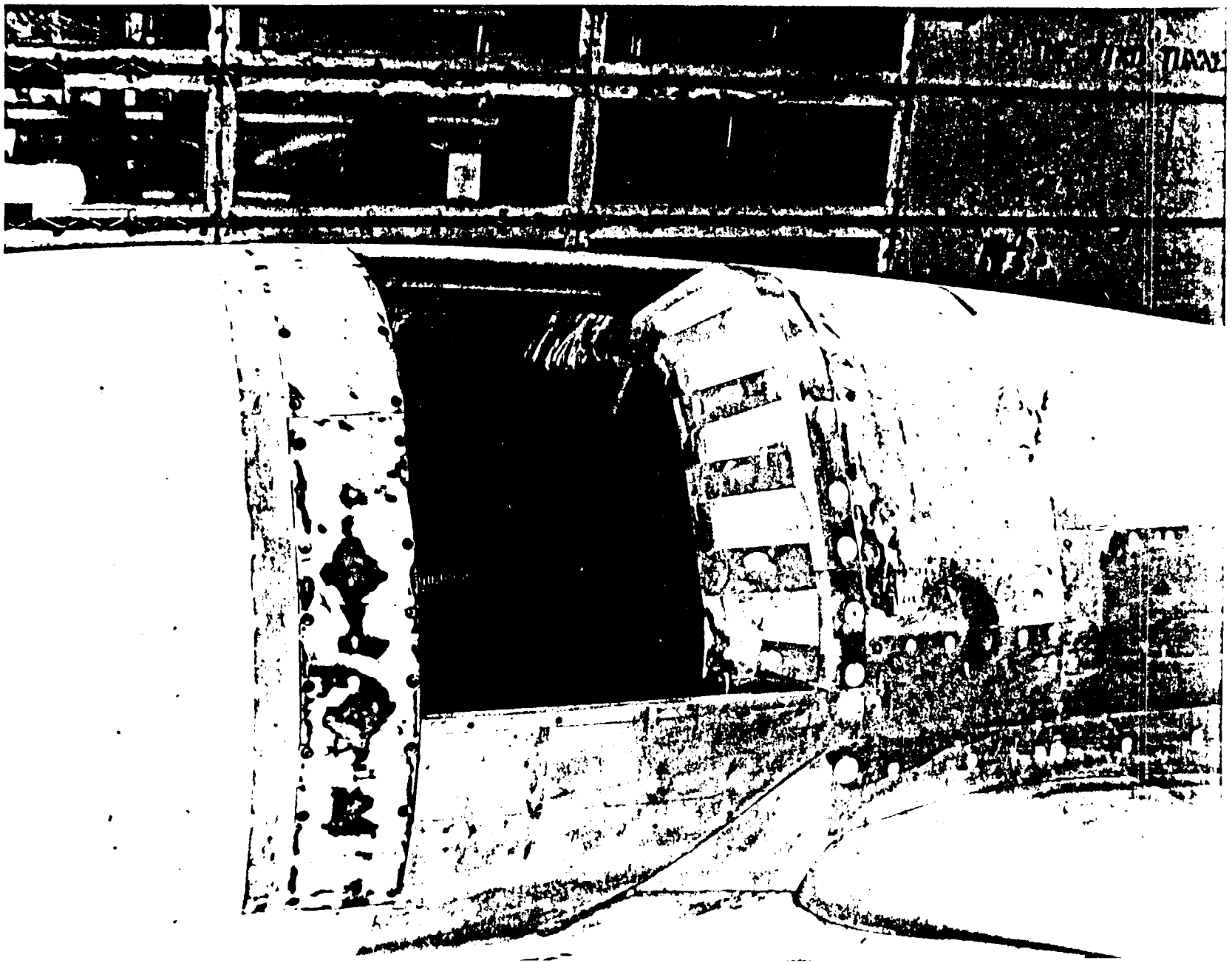

FIGURE 8. Photograph of the SOFIA model open cavity with a 30 degree, long aft ramp (Configuration 30).

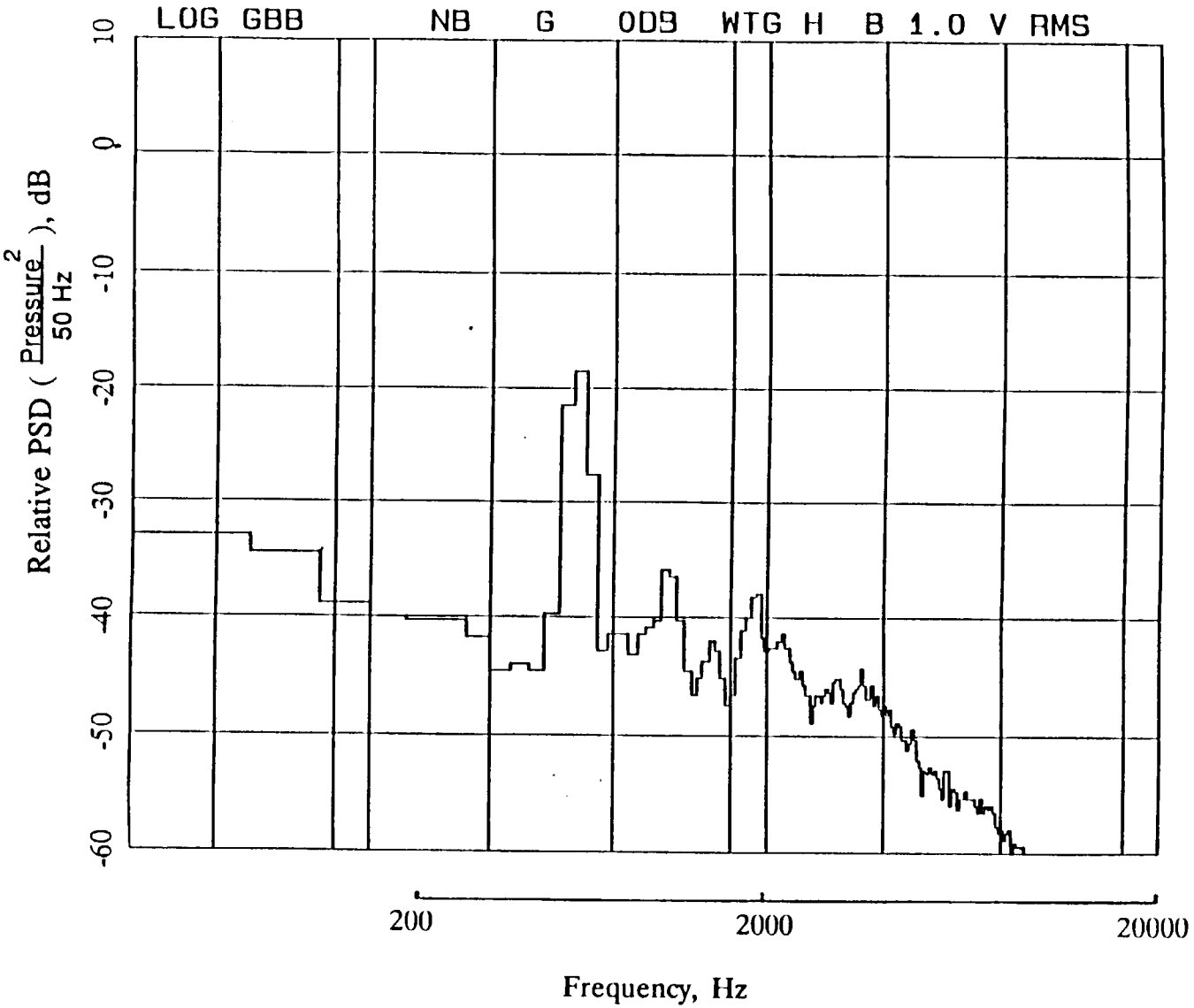

FIGURE 9. **Pressure fluctuation spectrum showing remnants of resonance for Configuration 30 at M = 0.85 and α = 2.5 degrees.**

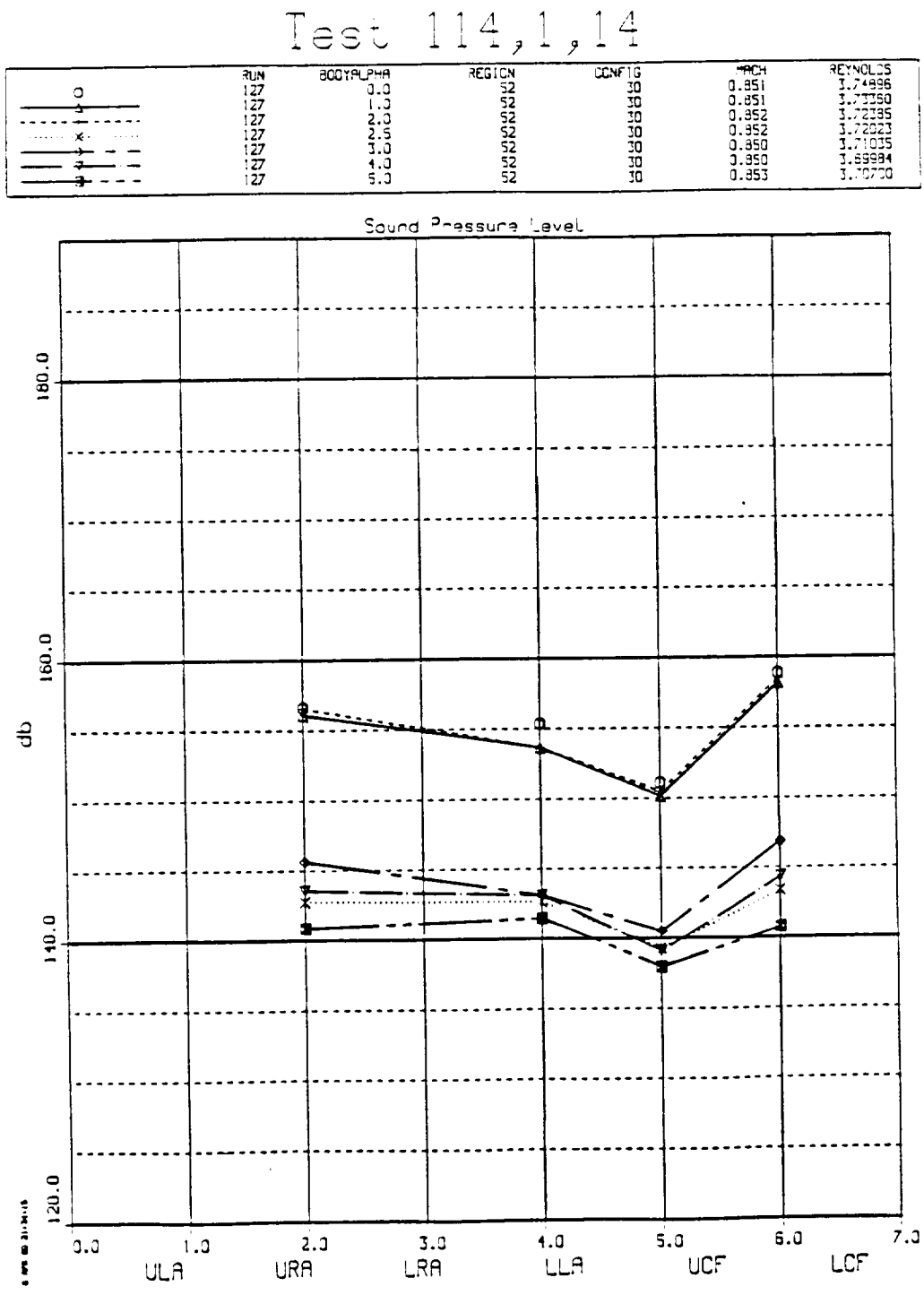

FIGURE 10. **Sound pressure level comparisons for the full aperture aft ramp treated cavity (Configuration 30) at various angles of attack for M = 0.85.**

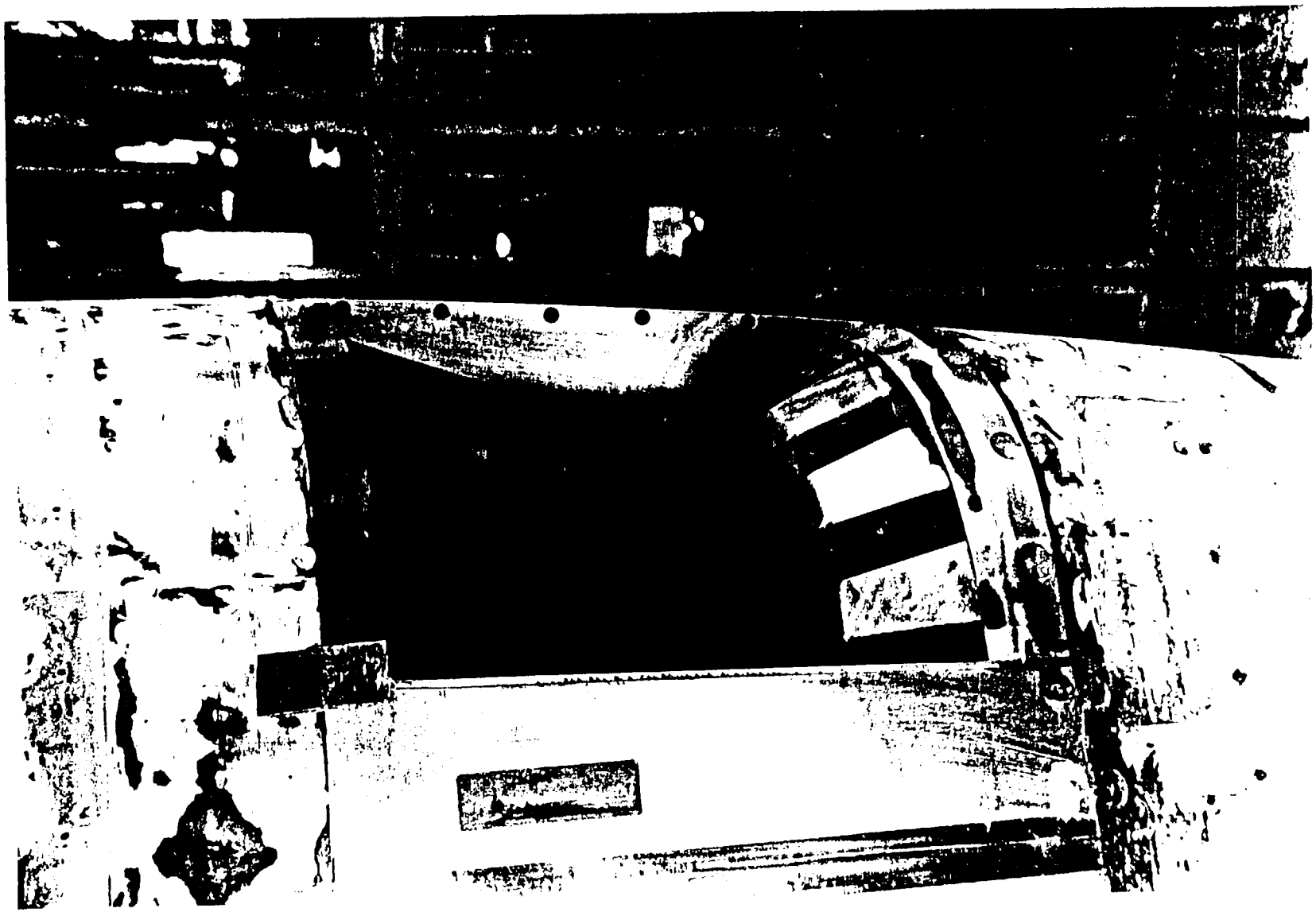

FIGURE 11. Photograph of the SOFIA model limited aperture high open cavity with aft ramp (Configuration 50).

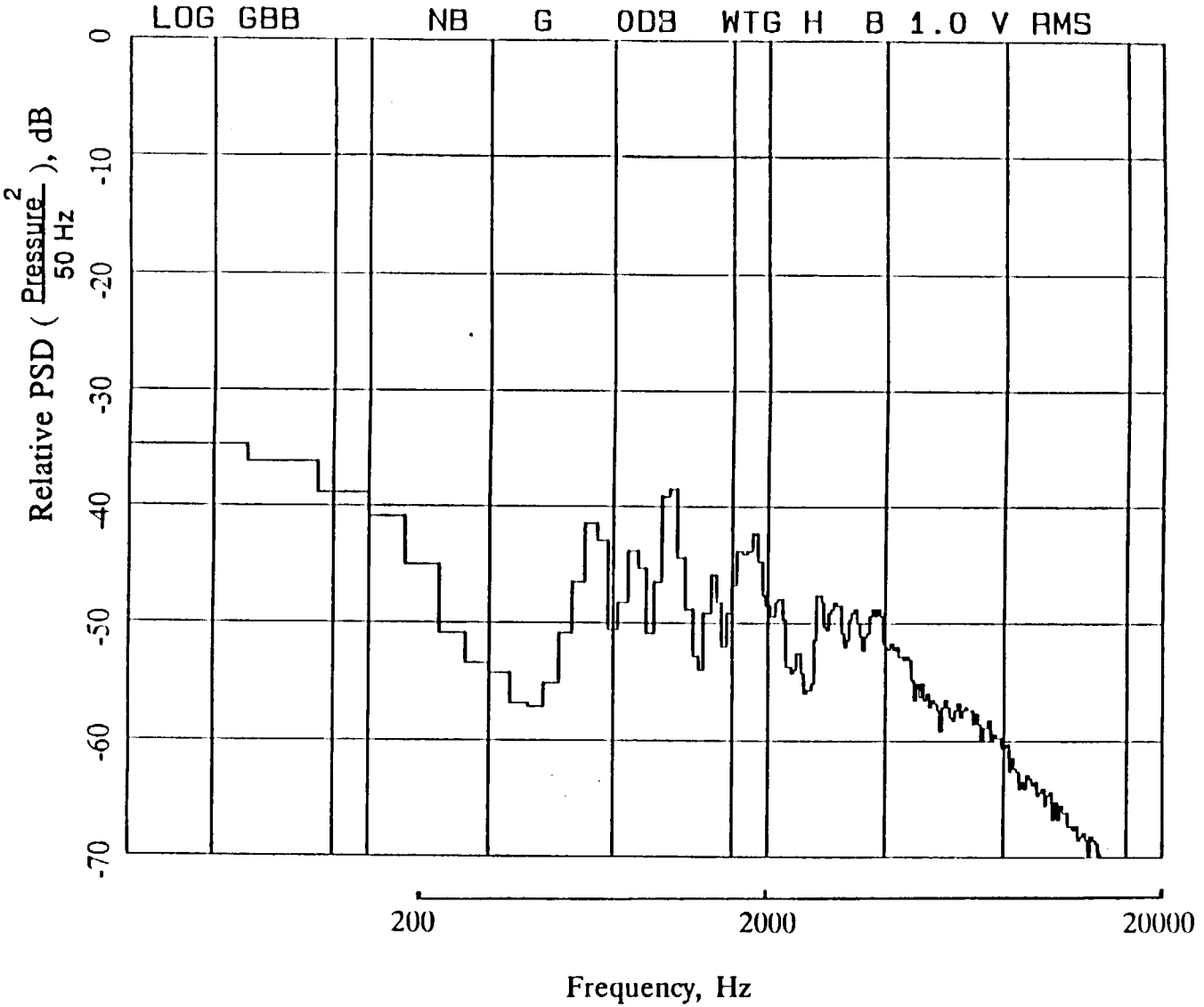

FIGURE 12. **Pressure fluctuation spectrum for Configuration 50 at M = 0.85 and α = 2.5 degrees.**

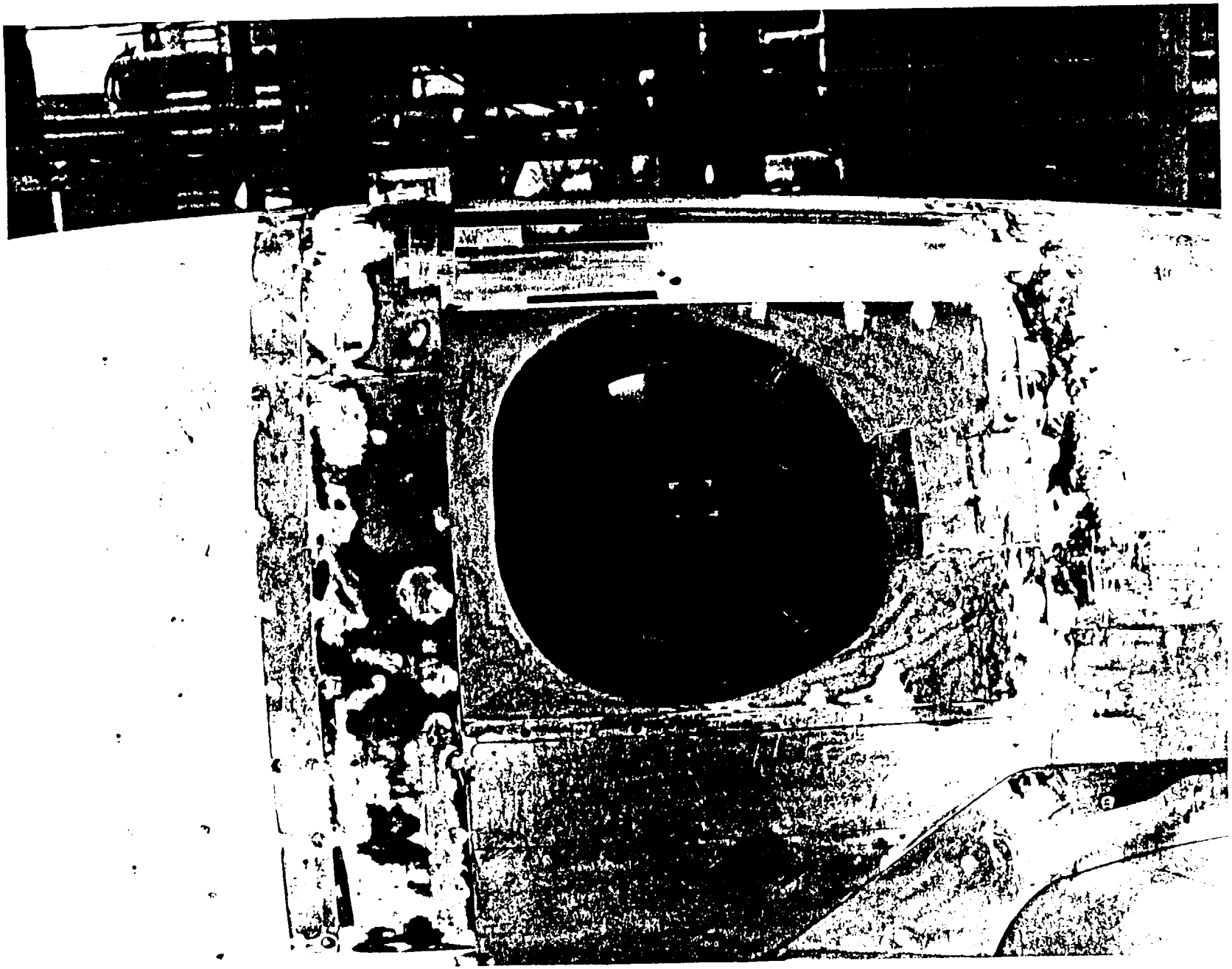

FIGURE 13. Photograph of the SOFIA model limited aperture low open cavity with moldings (Configuration 98).

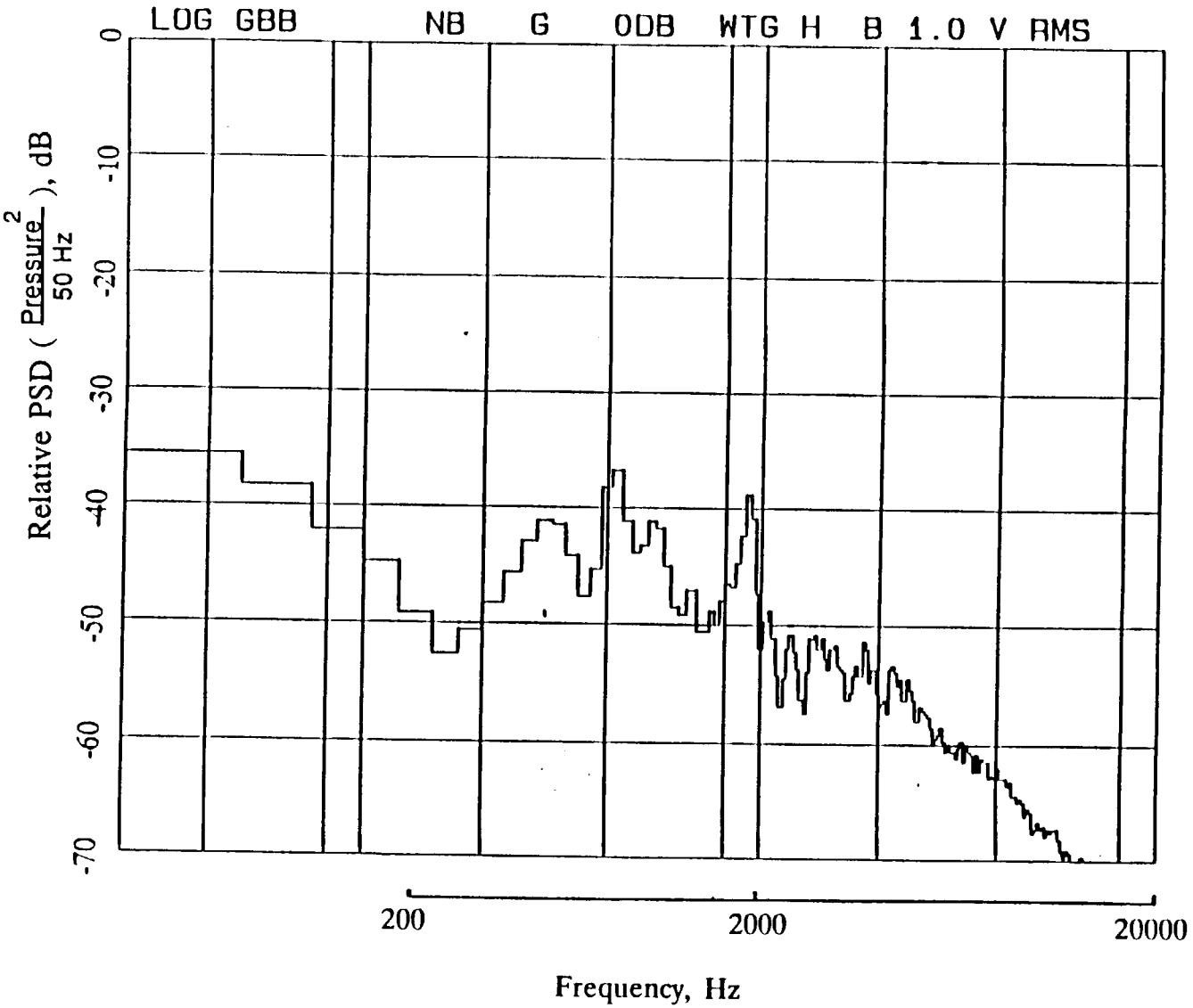

FIGURE 14. **Pressure fluctuation spectrum for Configuration 98 at M = 0.85 and α = 2.5 degrees.**

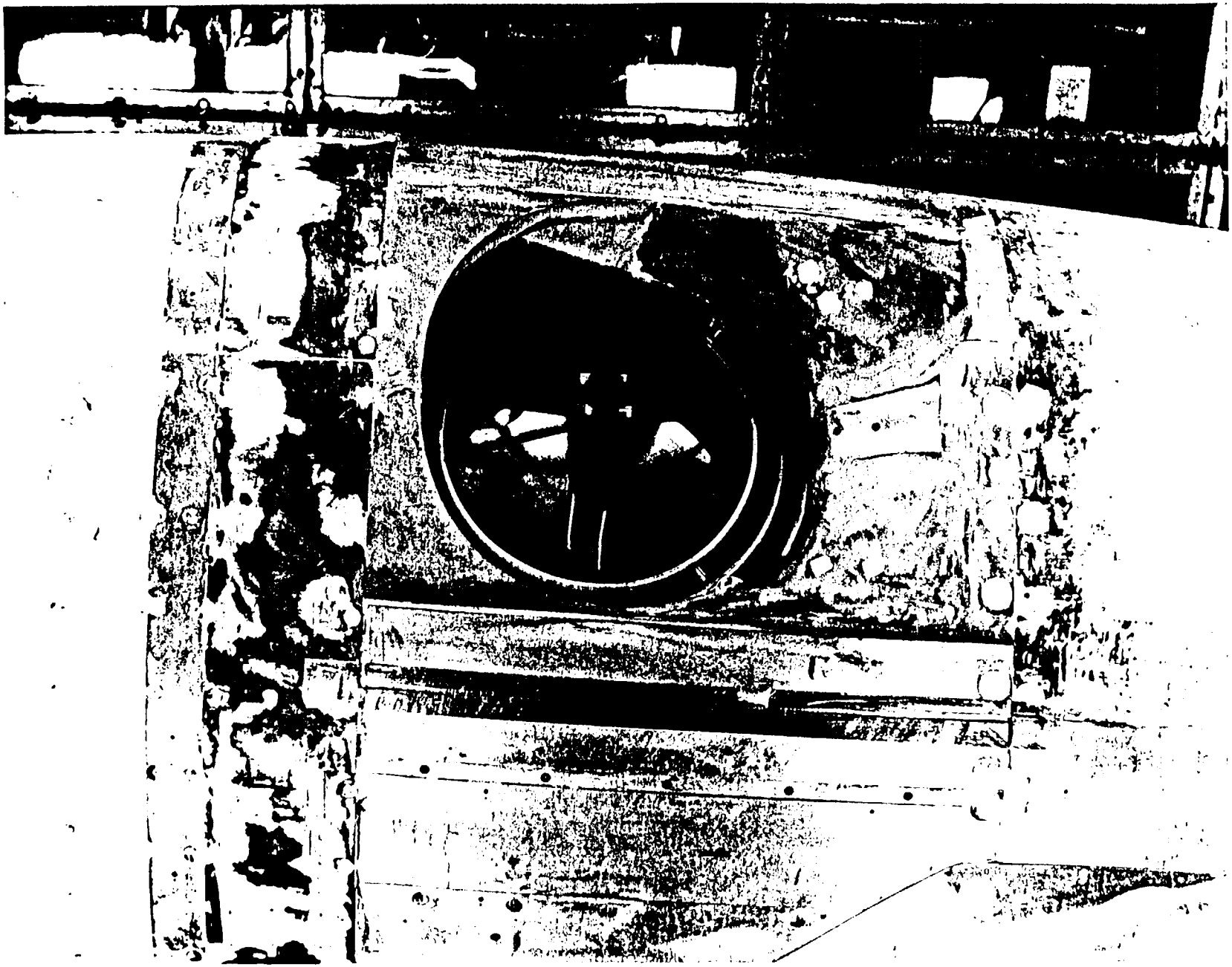

FIGURE 15. Photograph of the SOFIA model limited aperture mid open cavity with moldings (Configuration 100).

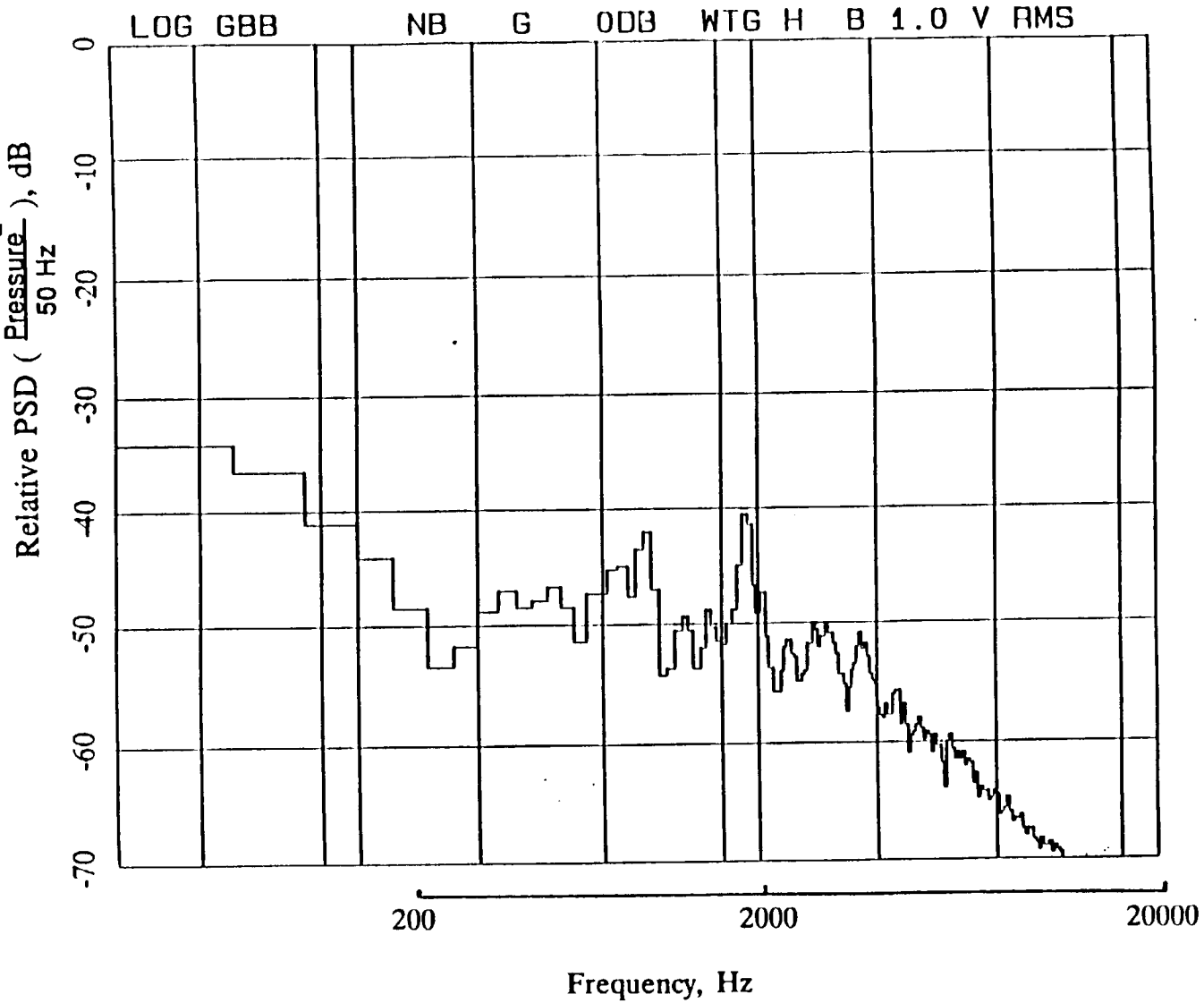

FIGURE 16. **Pressure fluctuation spectrum for Configuration 100 at M = 0.85 and α = 2.5 degrees.**

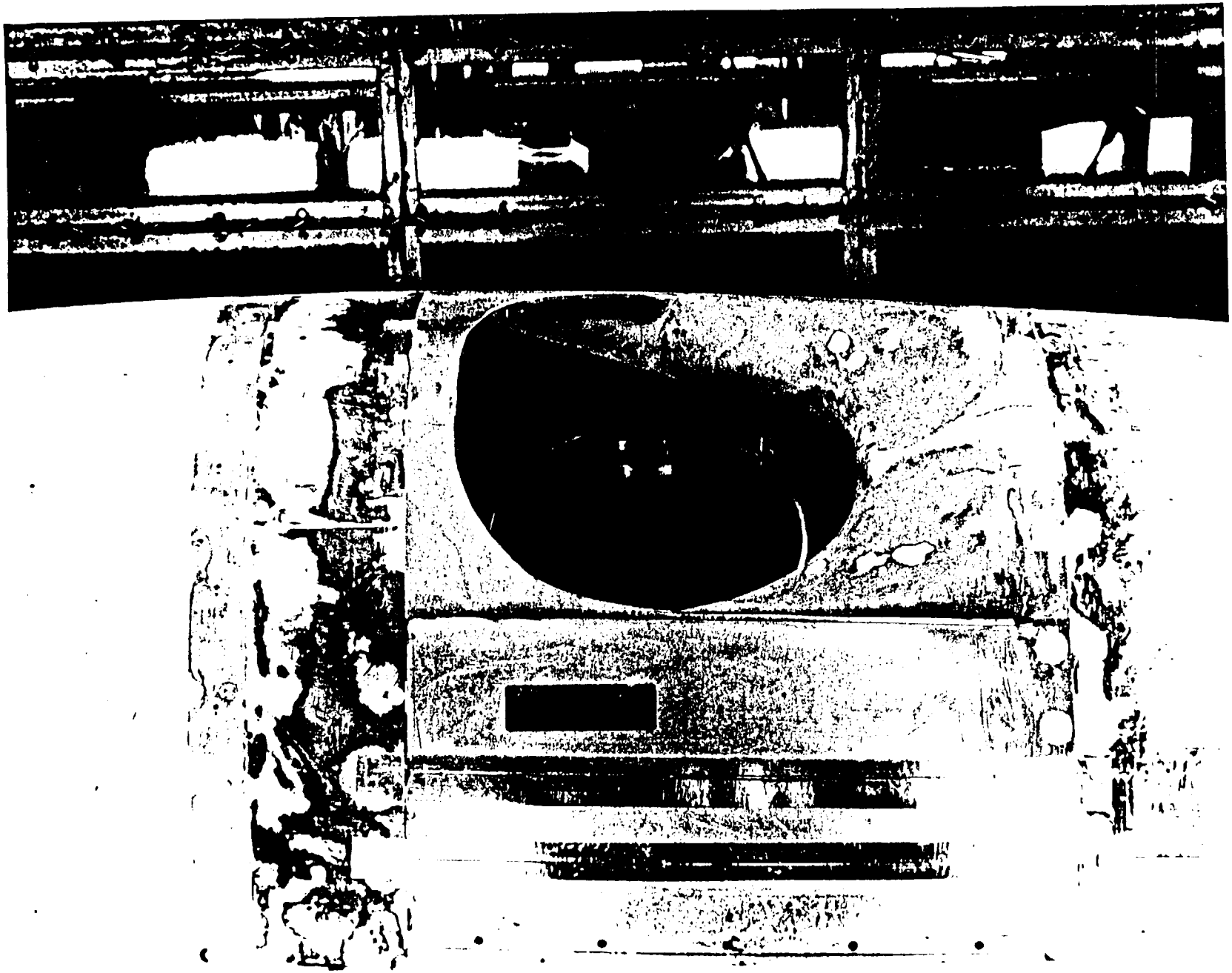

FIGURE 17. Photograph of the SOFIA model limited aperture high open cavity with moldings (Configuration 101).

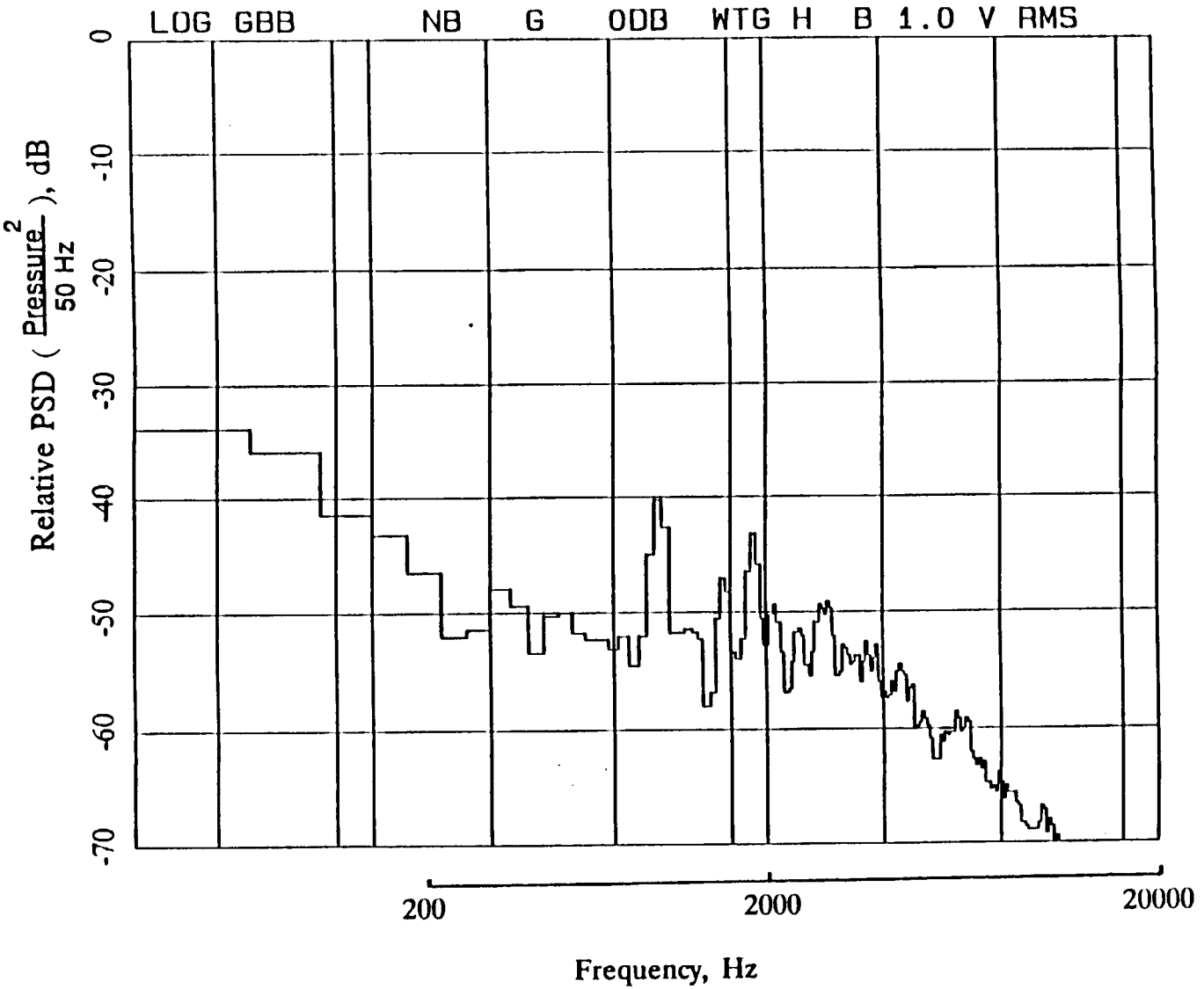

FIGURE 18. **Pressure fluctuation spectrum for Configuration 101 at M = 0.85 and α = 2.5 degrees.**

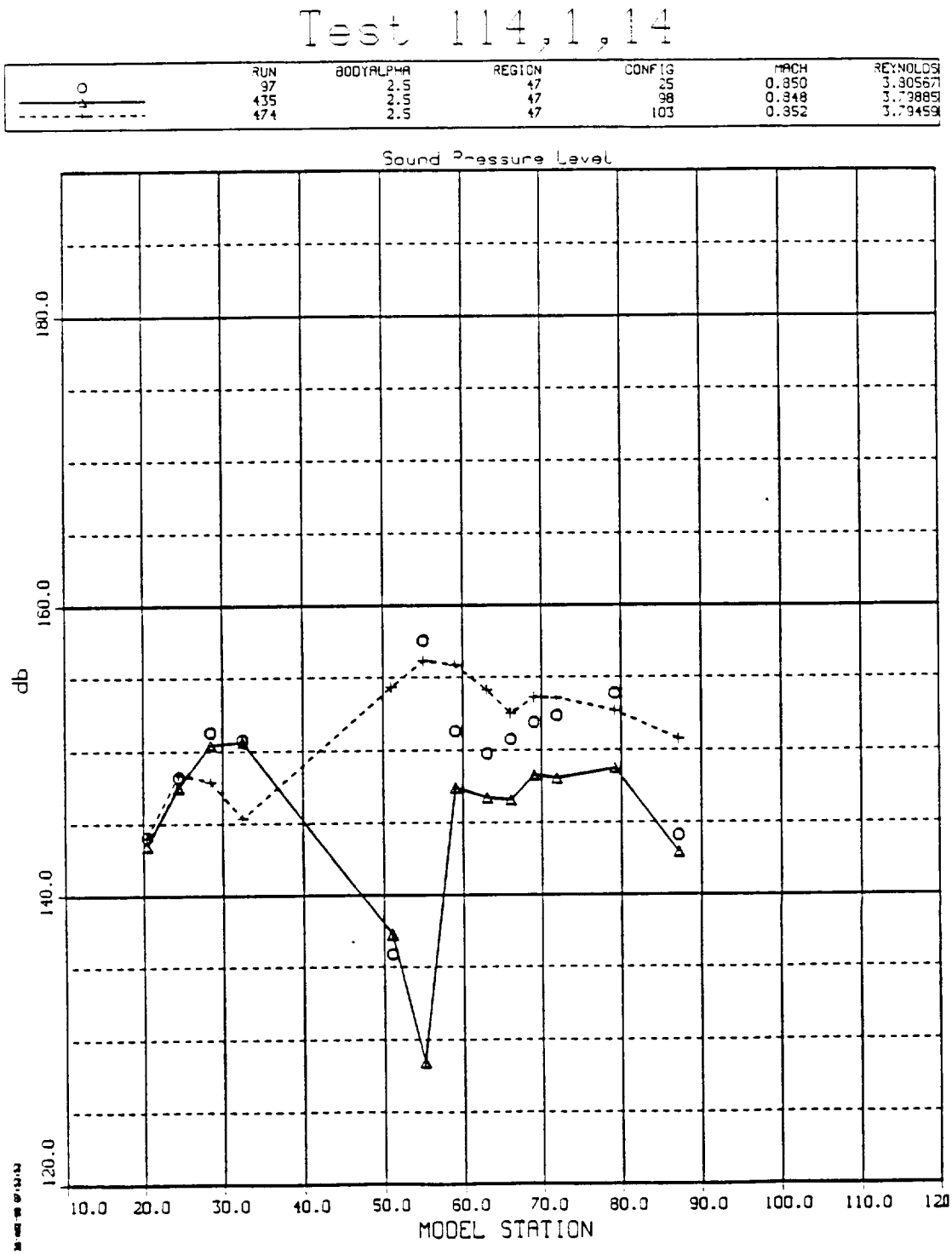

FIGURE 19. Sound pressure level comparisons upstream and downstream of resonating (Configuration 25), molding quieted (Configuration 98), and fence quieted (Configuration 103) cavities for M = 0.85 and α = 2.5 degrees on the lower portion of the model.

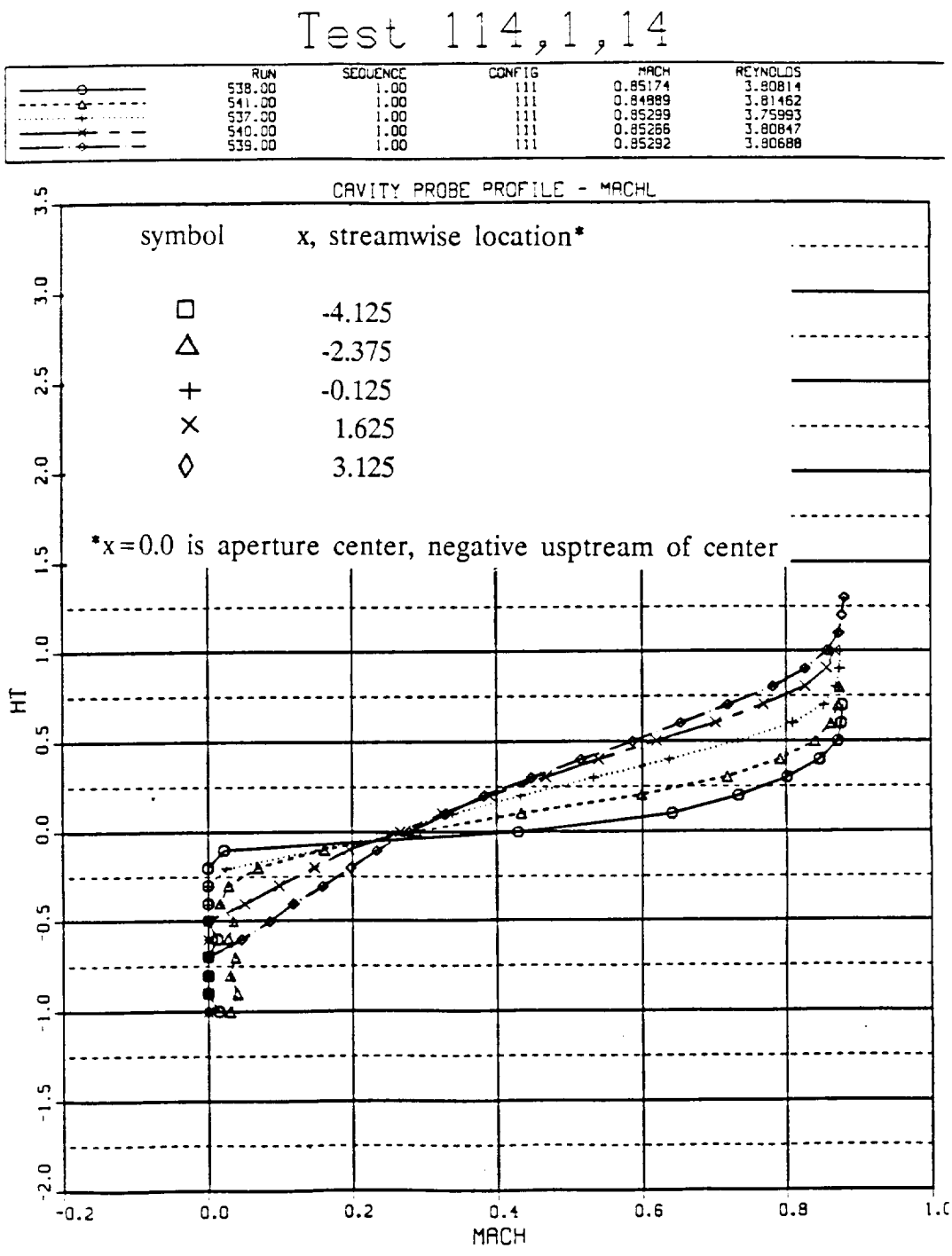

FIGURE 20. **Representative mean Mach number profiles obtained at several streamwise positions of the limited aperture mid (Configuration 111) cavity with moldings at M = 0.85 and α = 2.5 degrees.**

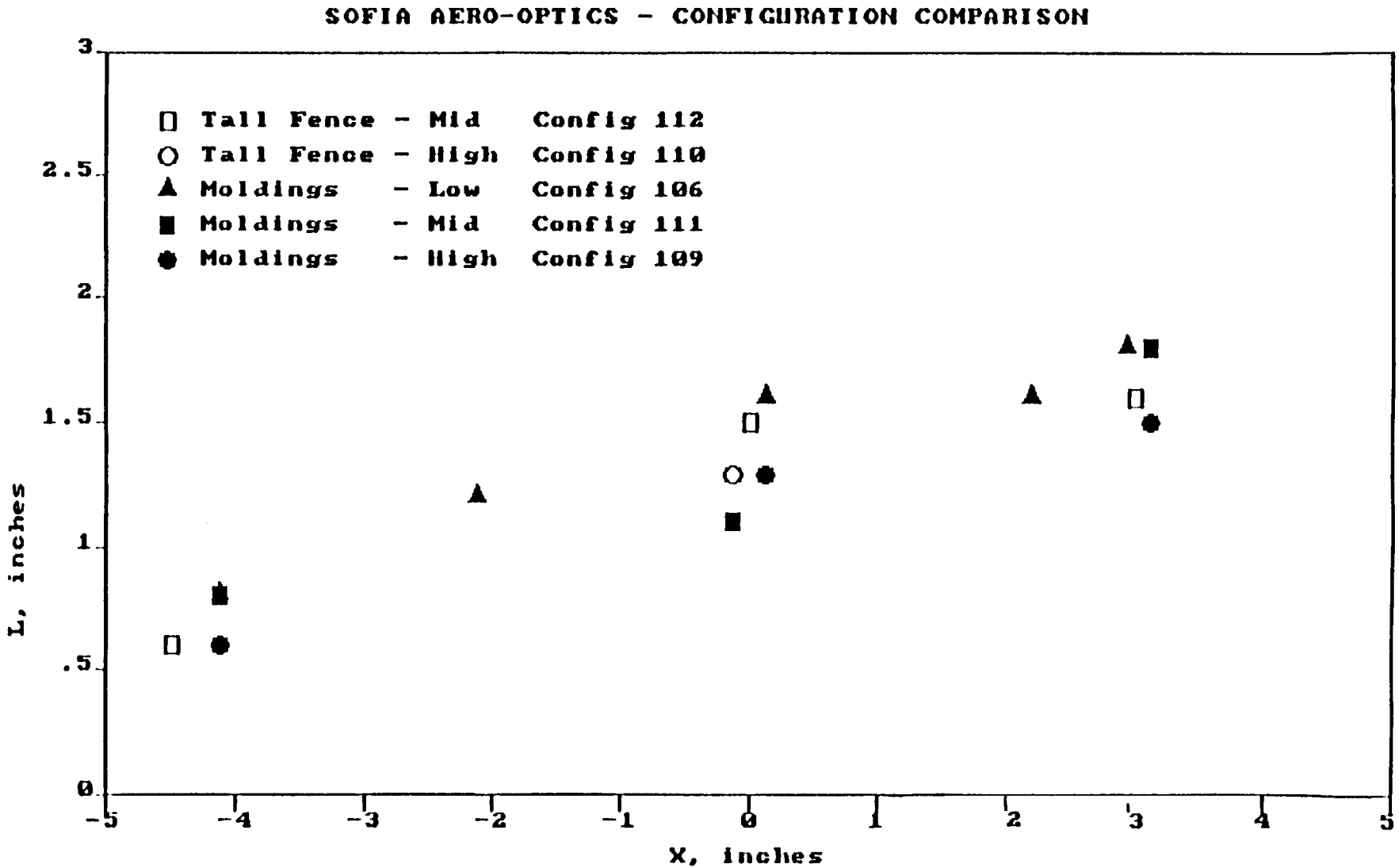

FIGURE 21. Comparison of shear layer width for fence and molded configurations.

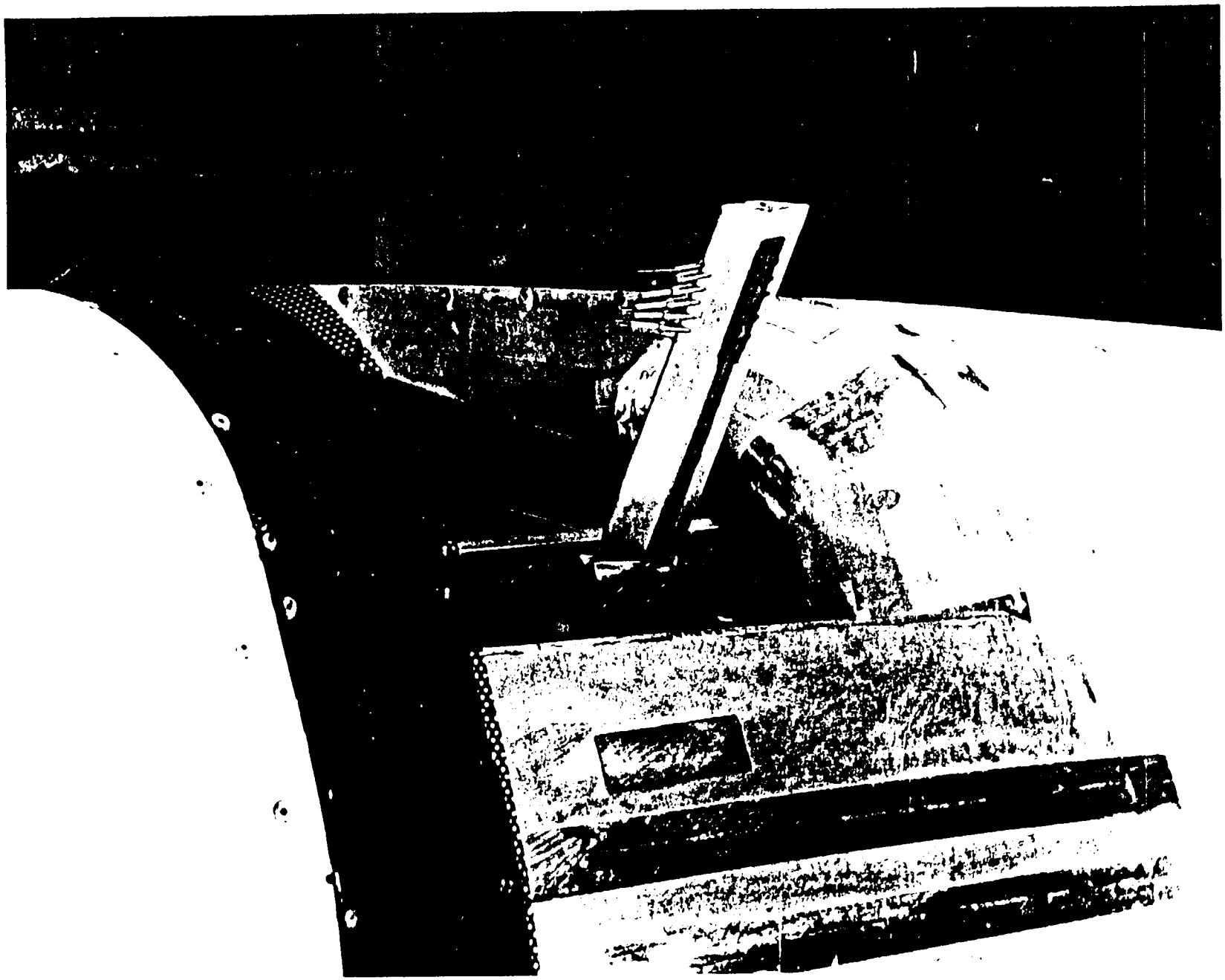

FIGURE 22. Photograph of rake and probe drive mounted in SOFIA model.

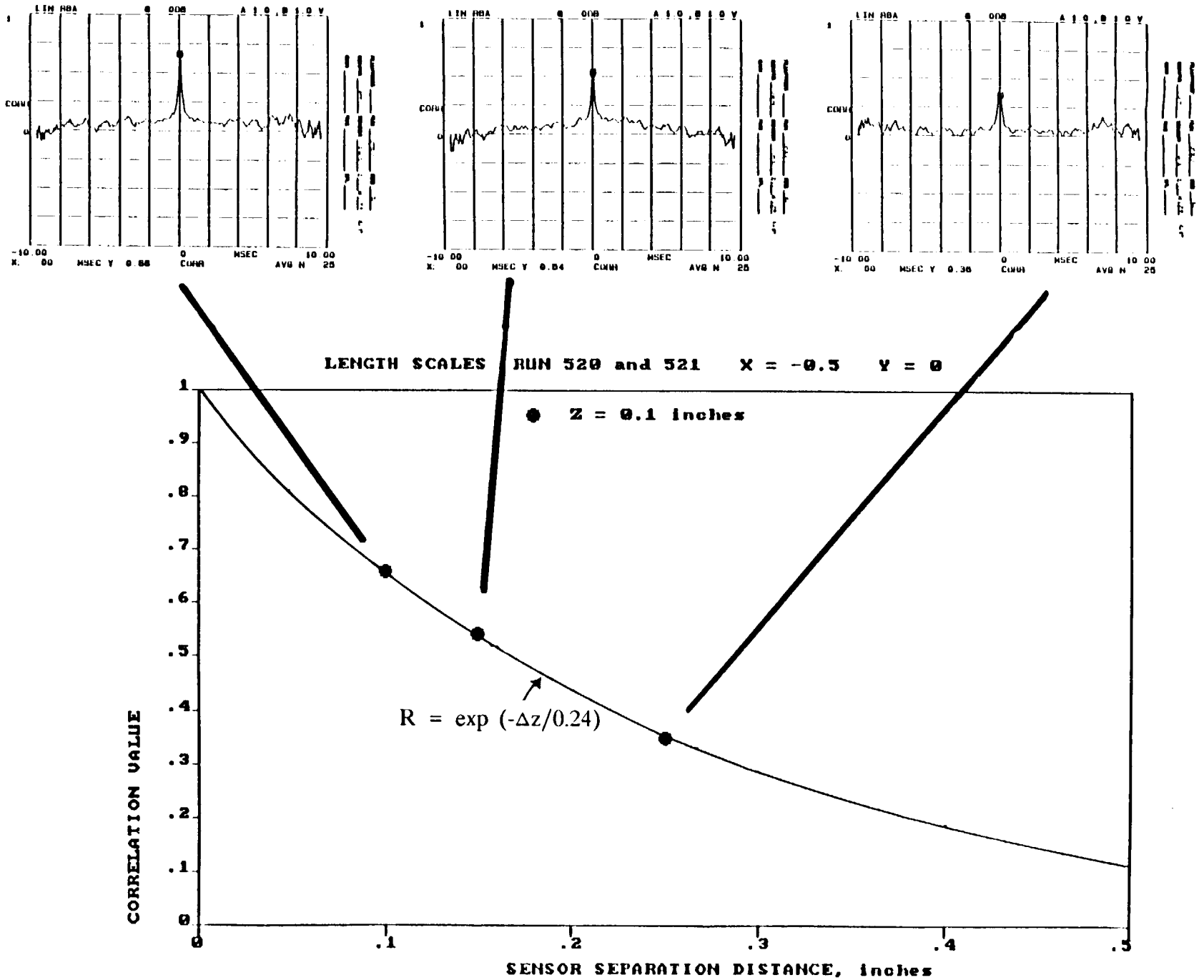

FIGURE 23. Representative spatial correlation function derived from three temporal correlation functions.

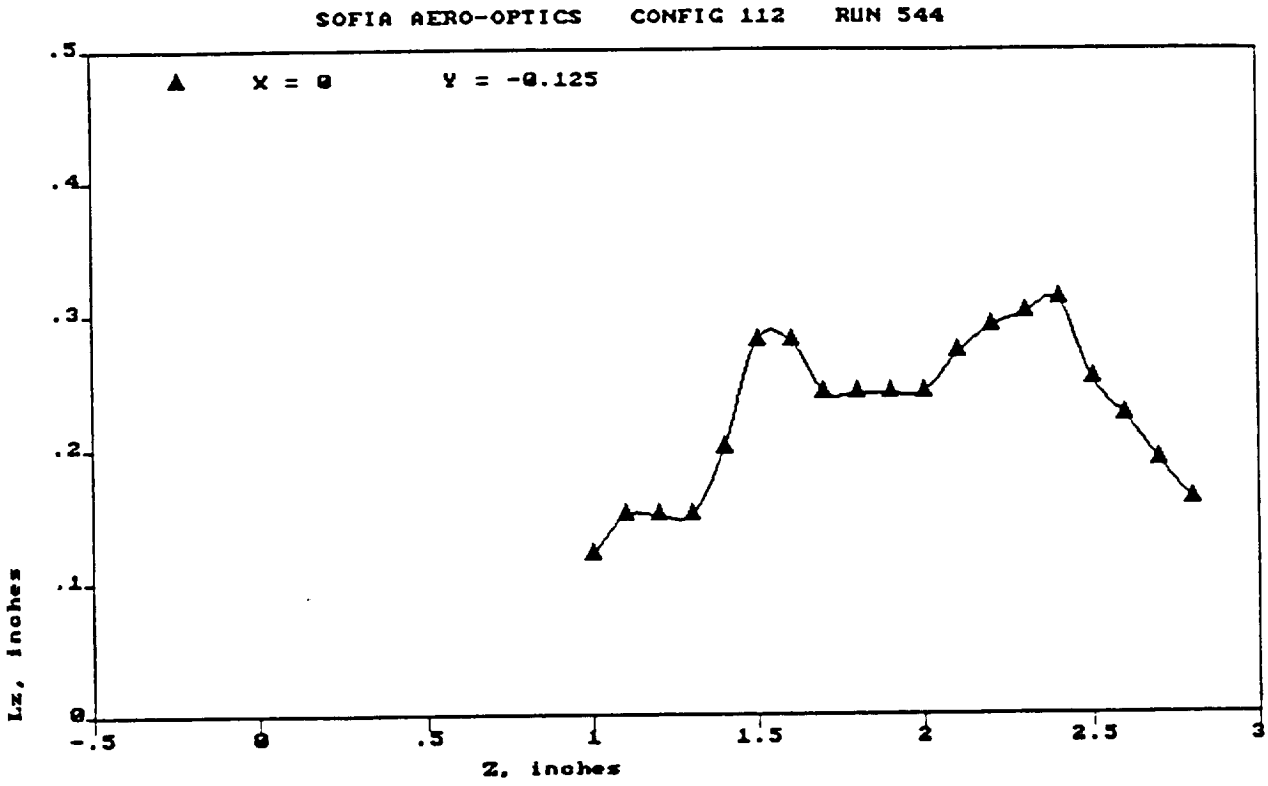

FIGURE 24. Representative integral scale length distribution through shear layer for fence quieted limited aperture mid (Configuration 112).

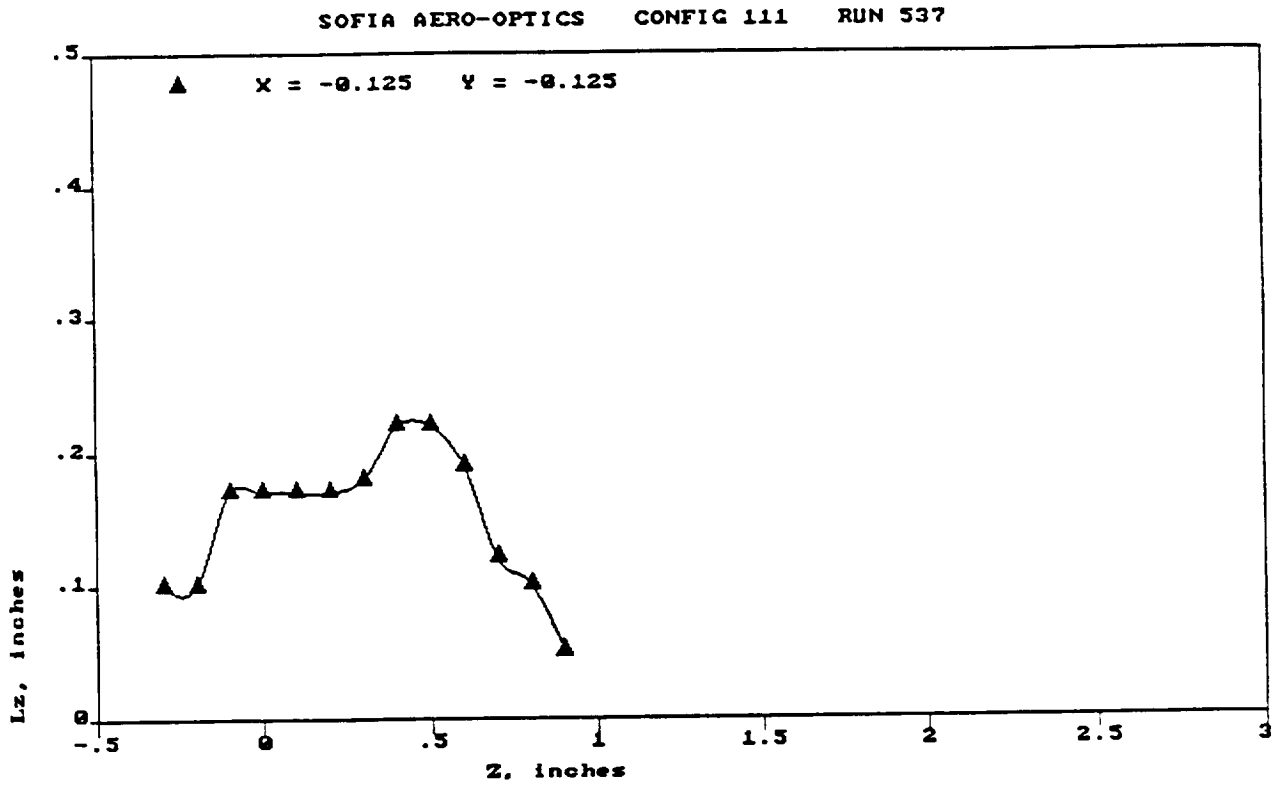

FIGURE 25. Representative integral scale length distribution through shear layer for molding quieted limited aperture mid (Configuration 111).

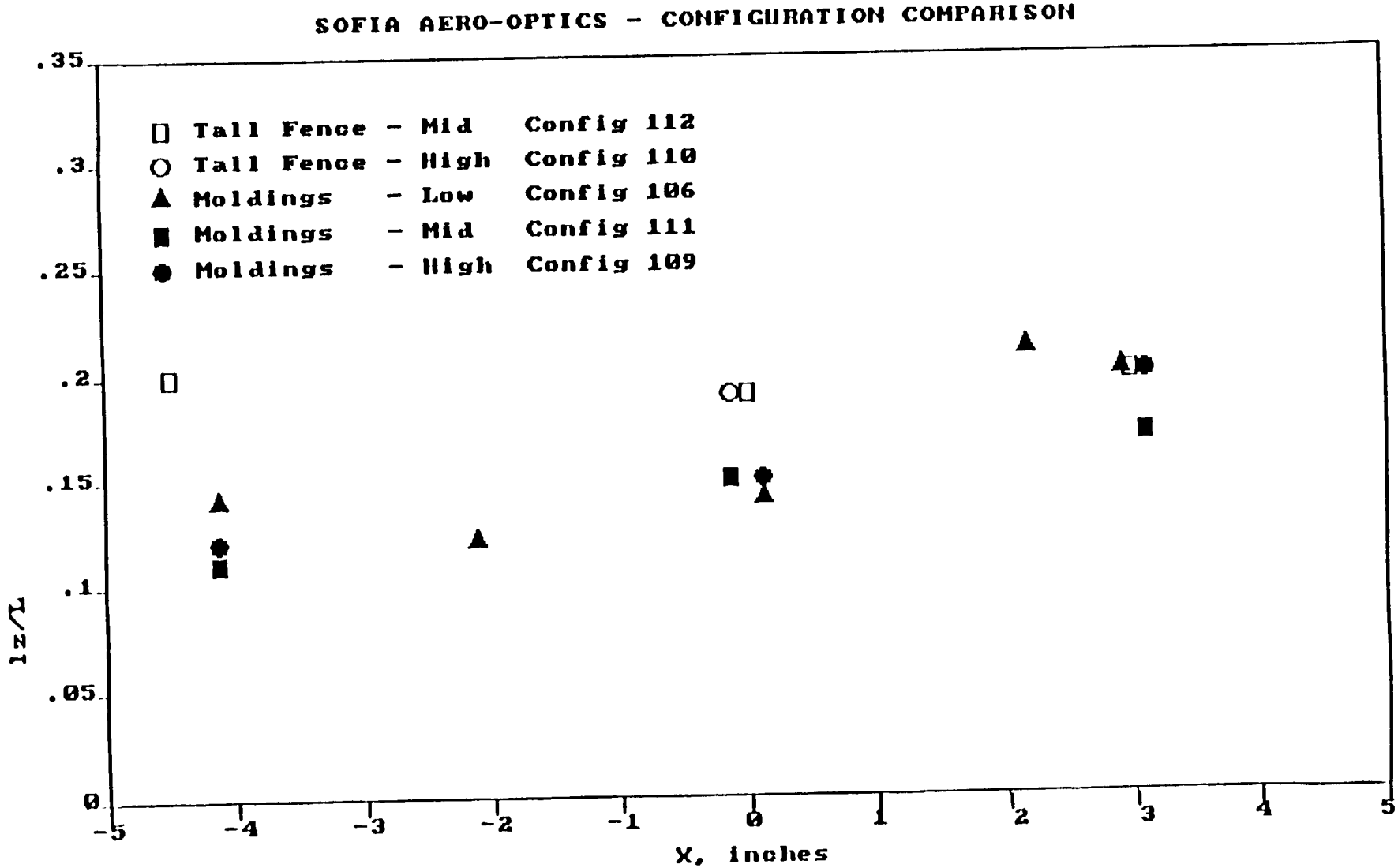

FIGURE 26. Ratio of scale size to shear layer width for fence and molded configurations.

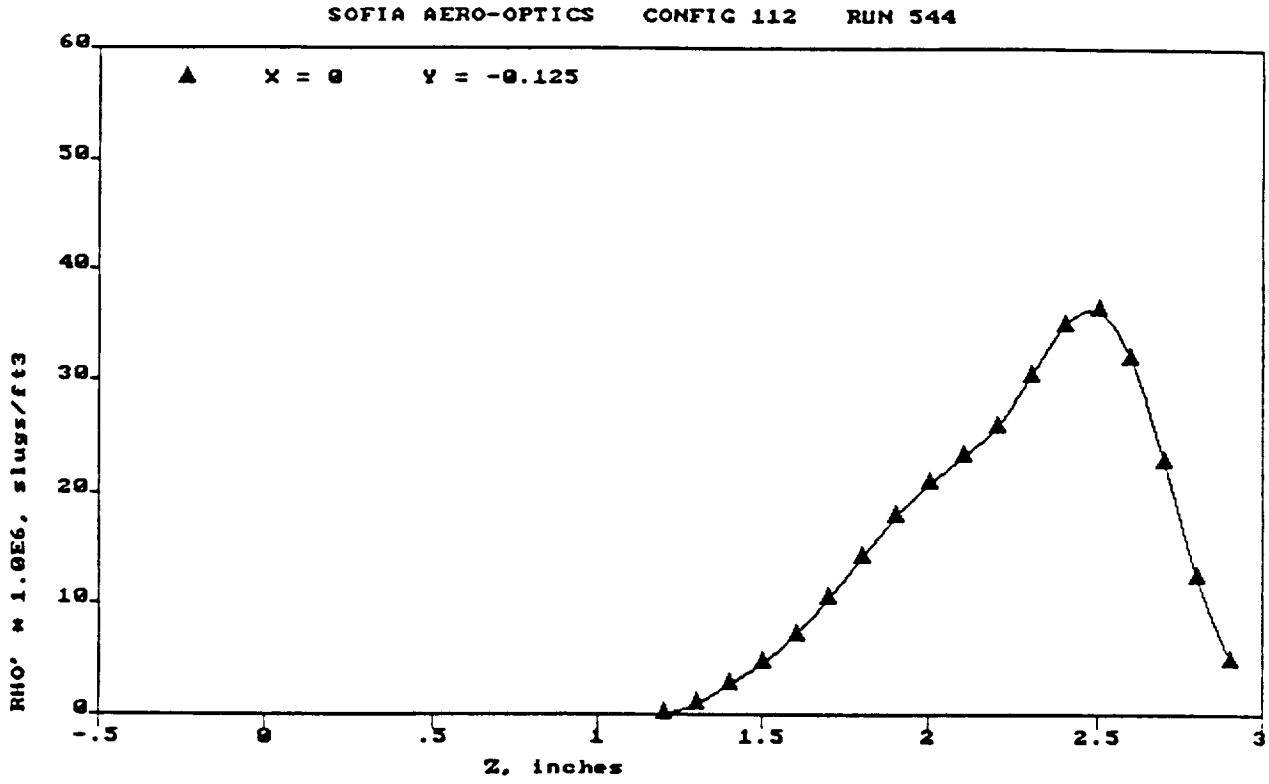

FIGURE 27. **Representative RMS density fluctuation distribution through shear layer for fence quieted limited aperture mid (Configuration 112).**

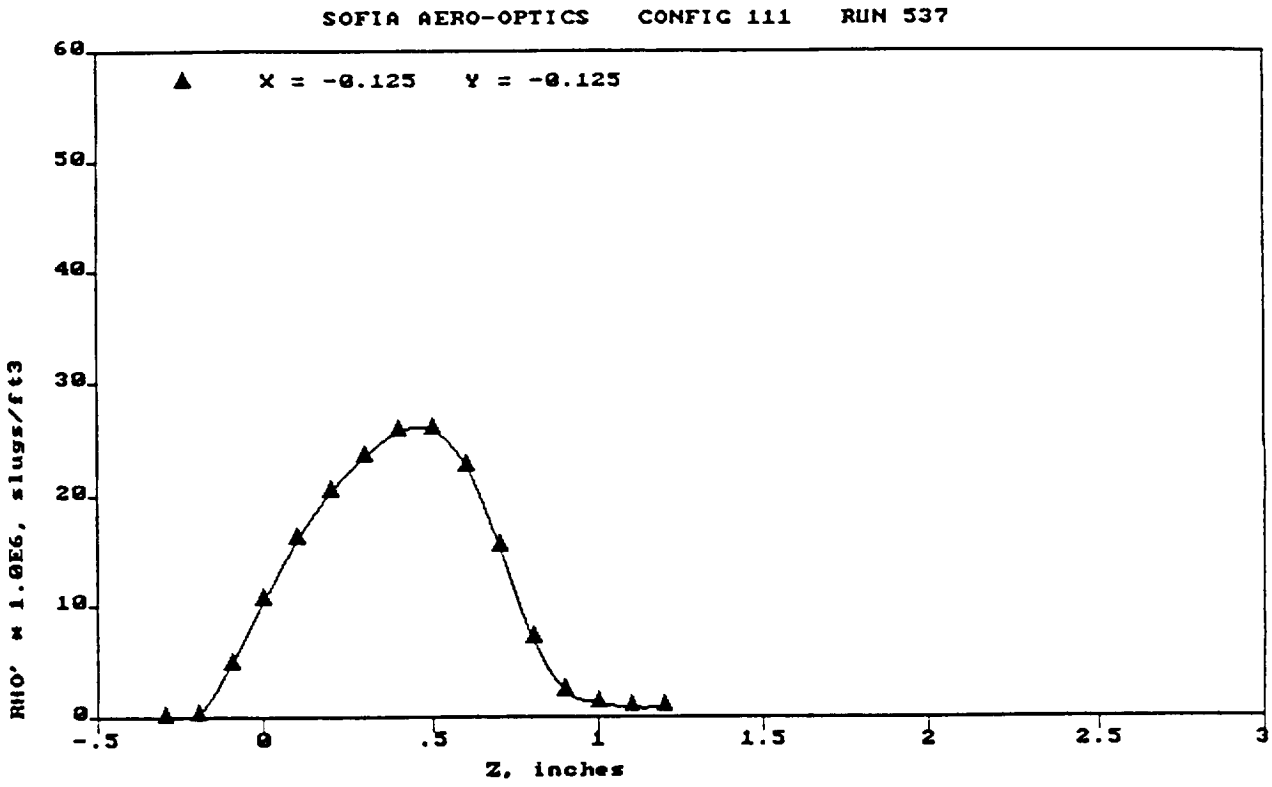

FIGURE 28. Representative RMS density fluctuation distribution through shear layer for molding quieted limited aperture mid (Configuration 111).

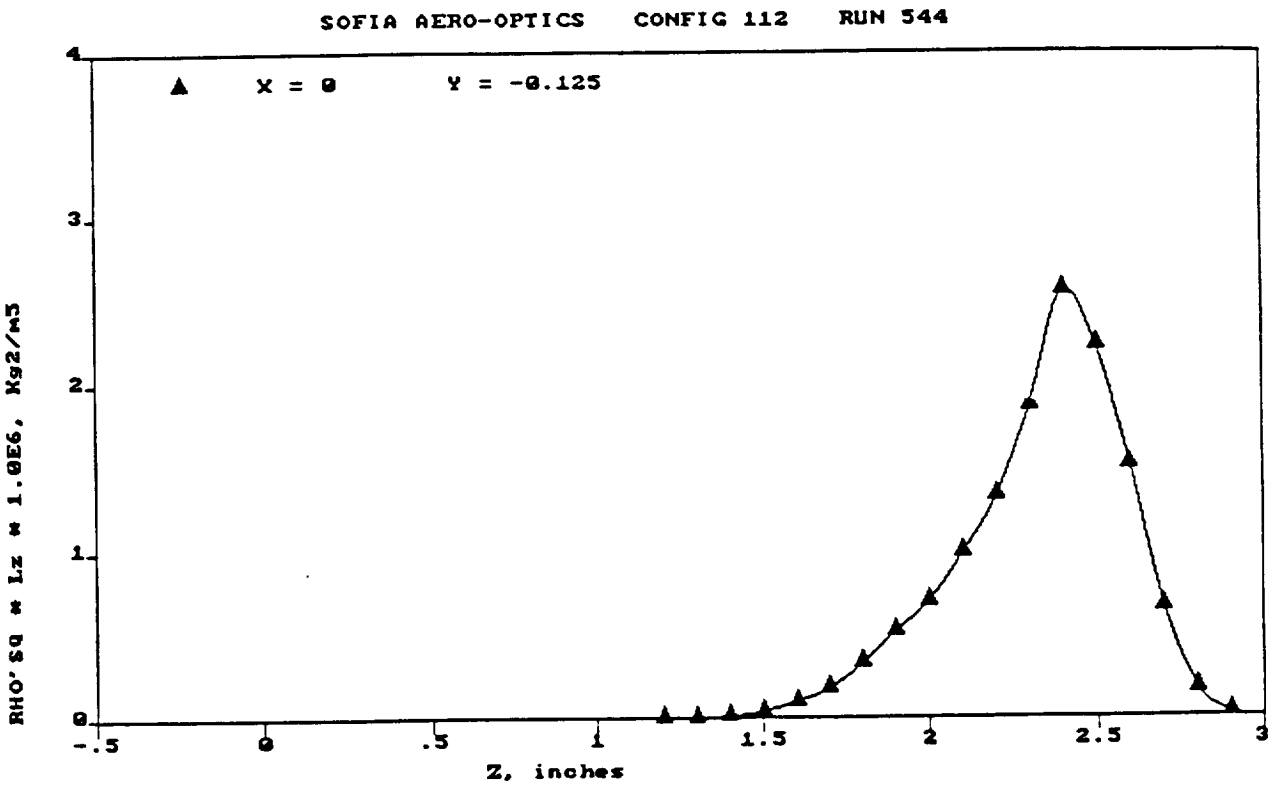

FIGURE 29. Representative aero-optical integrand distribution through shear layer for fence quieted limited aperture mid (Configuration 112).

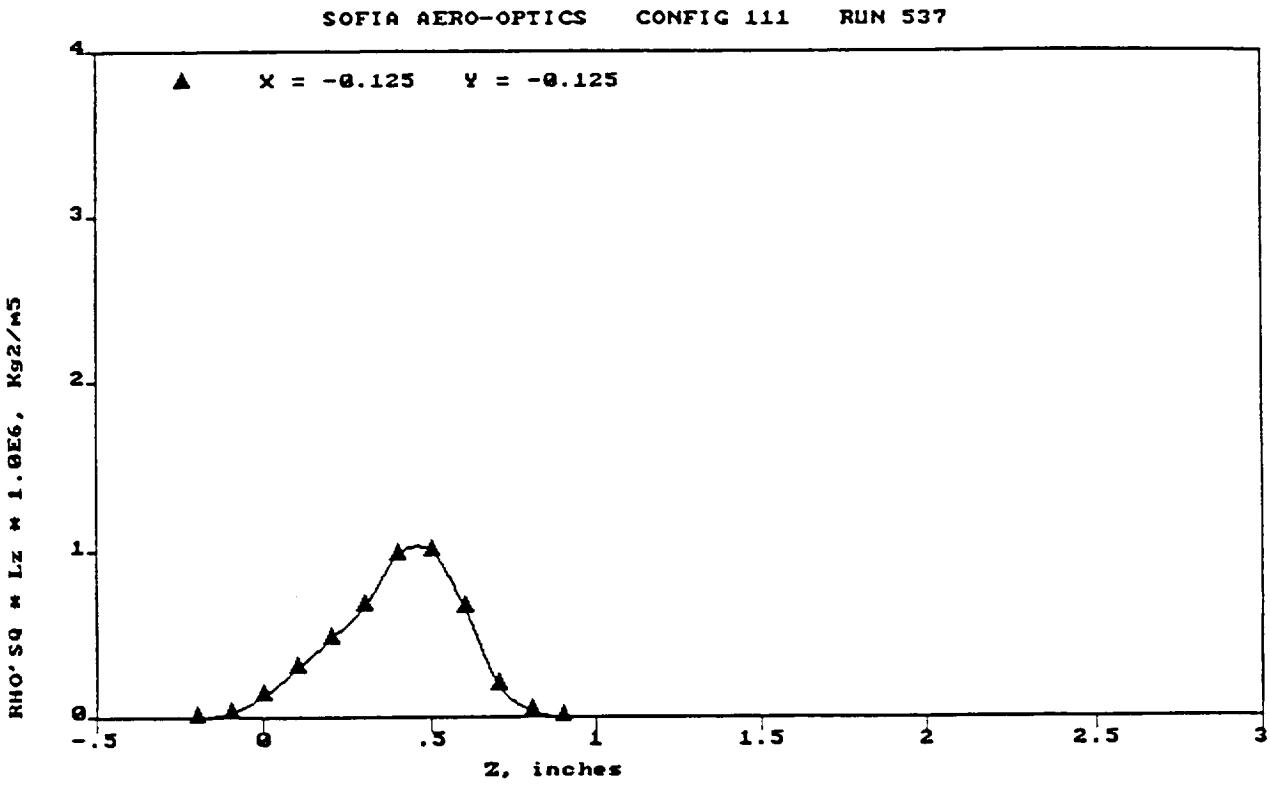

FIGURE 30. Representative aero-optical integrand distribution through shear layer for molding quieted limited aperture mid (Configuration 111).

SOFIA WIND TUNNEL AERO-OPTICS

CONFIG: 112
RUN NO: 544
MACH #: 0.85
ALPHA : 2.5 deg

X = 0
Y = -0.125

Z inches	Ebar3 volts	E'rms3 volts	MACH NO	FLU DEN slugs/ft3	RHO'*1.0E6 slugs/ft3	Lz inch	RHO'SQ*Lz Kg2/m5	SIGMA SQ meters2
1.0	3.75	0.381	0.000	0.00114	0.000000	0.10	0.000E+00	
1.1	3.88	0.383	0.000	0.00114	0.000000	0.15	0.000E+00	0.0000E+00
1.2	4.03	0.378	0.000	0.00114	0.000000	0.15	0.000E+00	0.0000E+00
1.3	4.18	0.370	0.079	0.00114	0.930675	0.20	1.169E-09	1.5712E-19
1.4	4.31	0.359	0.137	0.00115	2.643651	0.20	9.435E-09	1.5820E-18
1.5	4.45	0.356	0.184	0.00115	4.552792	0.28	3.918E-08	8.1136E-18
1.6	4.63	0.344	0.238	0.00116	7.078328	0.28	9.469E-08	2.6101E-17
1.7	4.78	0.338	0.298	0.00116	10.421168	0.24	1.759E-07	6.2464E-17
1.8	4.95	0.317	0.367	0.00117	14.186620	0.24	3.260E-07	1.2991E-16
1.9	5.14	0.289	0.440	0.00119	17.821478	0.24	5.145E-07	2.4286E-16
2.0	5.28	0.250	0.523	0.00120	20.753638	0.24	6.978E-07	4.0574E-16
2.1	5.40	0.217	0.606	0.00122	23.260780	0.27	9.861E-07	6.3200E-16
2.2	5.51	0.198	0.684	0.00124	26.016022	0.29	1.325E-06	9.4251E-16
2.3	5.59	0.189	0.765	0.00128	30.404105	0.30	1.872E-06	1.3721E-15
2.4	5.66	0.187	0.838	0.00130	34.884972	0.31	2.546E-06	1.9657E-15
2.5	5.73	0.175	0.896	0.00132	36.293198	0.25	2.223E-06	2.6066E-15
2.6	5.79	0.145	0.930	0.00134	31.946568	0.22	1.516E-06	3.1089E-15
2.7	5.85	0.100	0.952	0.00135	22.740742	0.19	6.632E-07	3.4016E-15
2.8	5.87	0.054	0.959	0.00135	12.370216	0.16	1.653E-07	3.5130E-15
2.9	5.88	0.021	0.963	0.00135	4.831741	0.16	2.521E-08	3.5385E-15

AERODYNAMIC WAVEFRONT ERROR

SIGMA = 5.949E-08 ,meters

SIGMA = 0.059 ,microns

SIGMA/= IAMDA 0.112 ,wave

FIGURE 31. Tabulated aero-optical data for a representative fence configuration (112) near the center of the aperture.

SOFIA WIND TUNNEL AERO-OPTICS

CONFIG: 111
RUN NO: 537 X = -0.125
MACH #: 0.85 Y = -0.125
ALPHA : 2.5 deg

Z inches	Ebar3 volts	E'rms3 volts	MACH NO	FLU DEN slugs/ft3	RHO'*1.0E6 slugs/ft3	Lz inch	RHO'SQ*Lz Kg2/m5	SIGMA SQ meters2
-0.3	3.66	0.405	0.000	0.00126	0.000000	0.10	0.000E+00	
-0.2	3.99	0.458	0.026	0.00127	0.145956	0.10	1.438E-11	1.9321E-21
-0.1	4.32	0.467	0.154	0.00127	4.778307	0.17	2.620E-08	3.5242E-18
0.0	4.65	0.433	0.248	0.00127	10.516791	0.17	1.269E-07	2.4098E-17
0.1	4.91	0.379	0.338	0.00128	15.991574	0.17	2.935E-07	8.0581E-17
0.2	5.17	0.315	0.433	0.00129	20.308369	0.17	4.733E-07	1.8360E-16
0.3	5.37	0.254	0.533	0.00131	23.417378	0.18	6.663E-07	3.3672E-16
0.4	5.52	0.204	0.638	0.00134	25.681588	0.22	9.794E-07	5.5784E-16
0.5	5.64	0.163	0.733	0.00137	25.941025	0.22	9.993E-07	8.2372E-16
0.6	5.76	0.122	0.809	0.00139	22.623381	0.19	6.564E-07	1.0462E-15
0.7	5.85	0.077	0.851	0.00141	15.439286	0.12	1.931E-07	1.1603E-15
0.8	5.88	0.034	0.869	0.00142	7.054939	0.10	3.360E-08	1.1908E-15
0.9	5.91	0.011	0.873	0.00142	2.286952	0.05	1.765E-09	1.1955E-15
1.0	5.90	0.006	0.875	0.00141	1.245100	0.00	0.000E+00	1.1958E-15
1.1	5.91	0.004	0.862	0.00145	0.832796	0.00	0.000E+00	1.1958E-15
1.2	5.91	0.004	0.864	0.00145	0.835775	0.00	0.000E+00	1.1958E-15

AERODYNAMIC WAVEFRONT ERROR

SIGMA = 3.458E-08 ,meters

SIGMA = 0.035 ,microns

SIGMA/= LAMDA 0.065 ,wave

FIGURE 32. Tabulated aero-optical data for a representative molded configuration (111) near the center of the aperture.

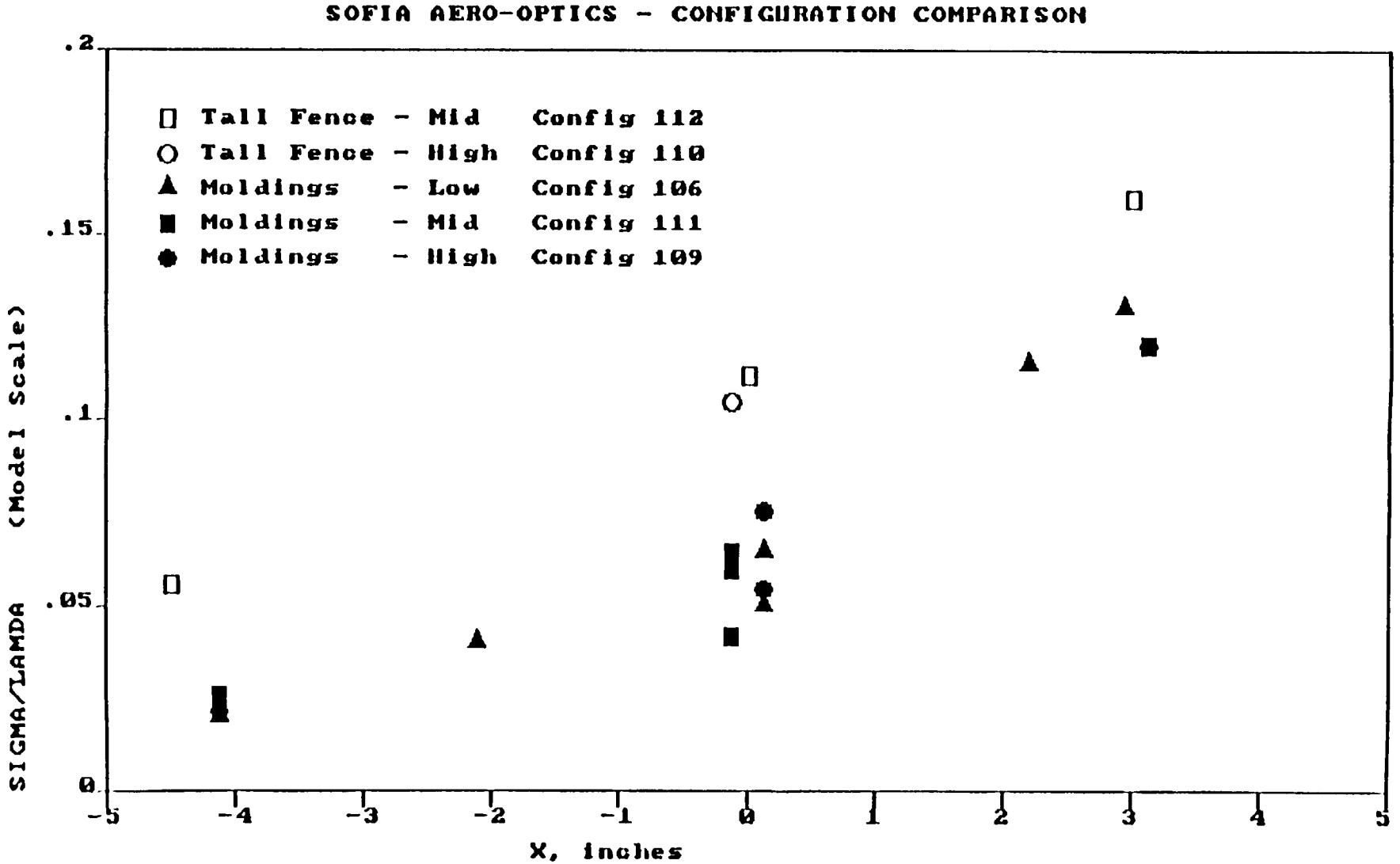

FIGURE 33. Variation of wind tunnel wavefront error over the aperture for fence and molded configurations.

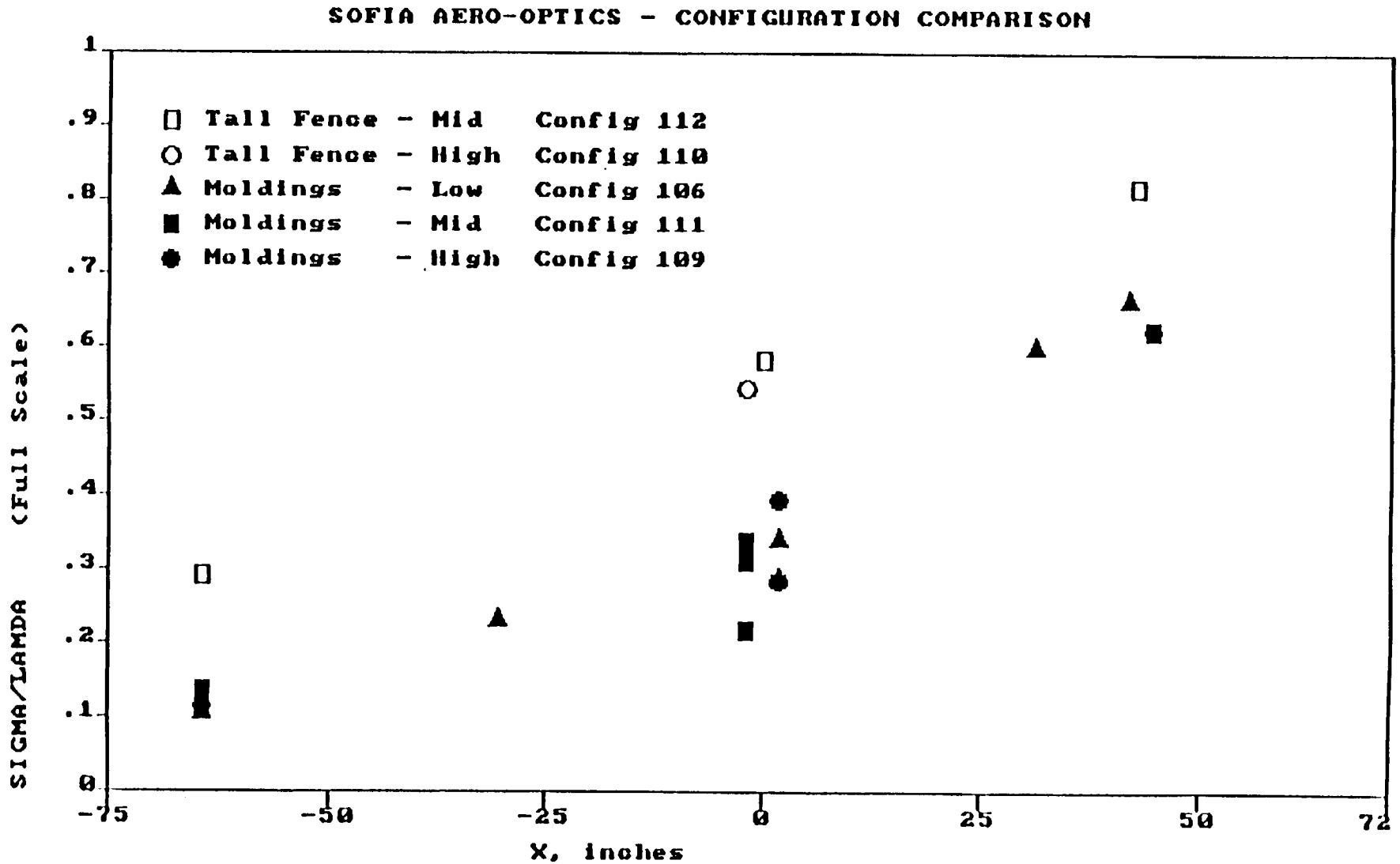

FIGURE 34. Variation of full-scale wavefront error over the aperture for fence and molded configurations at M = 0.85 and α = 2.5 degrees and 41,000 feet.

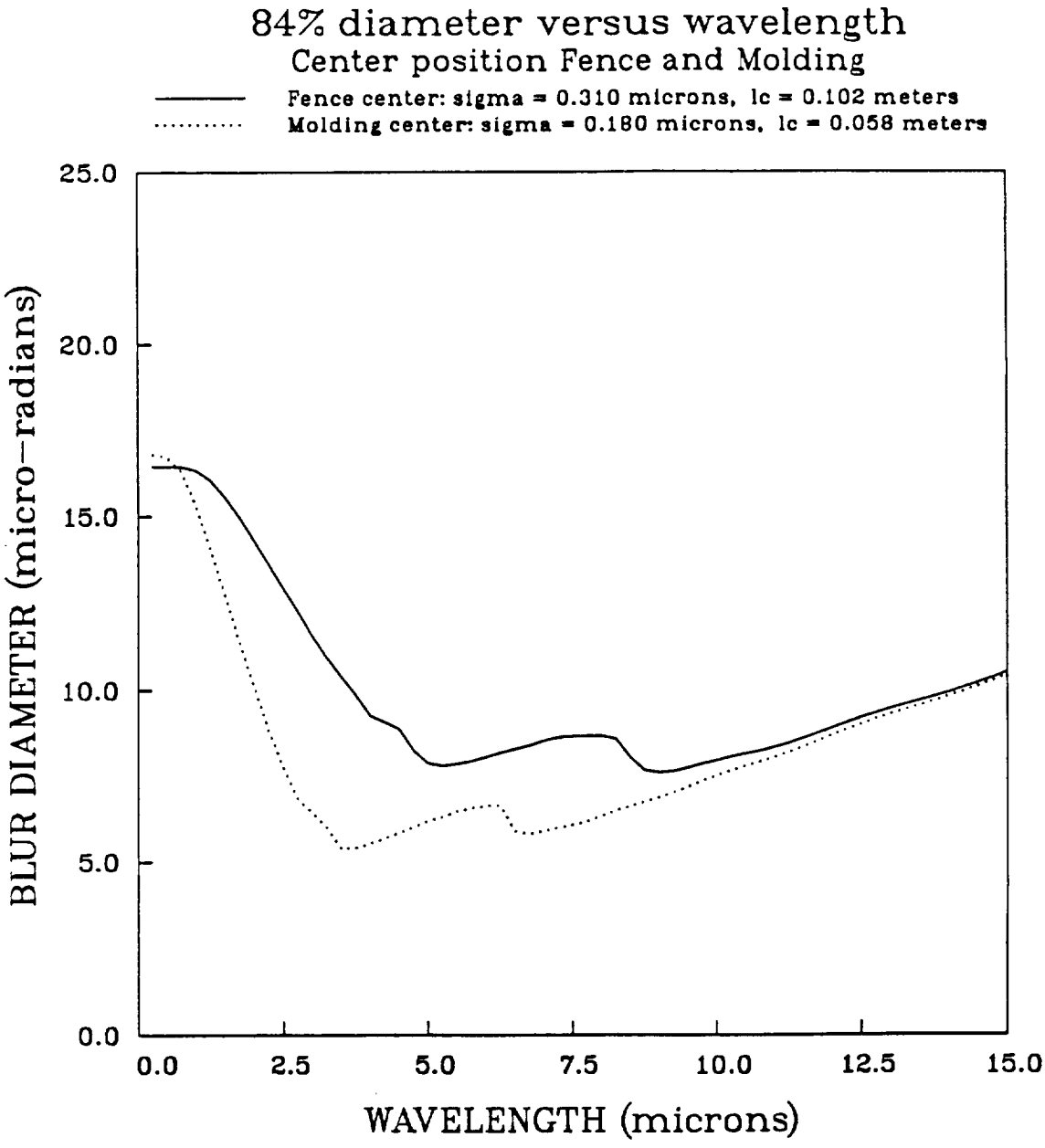

FIGURE 35. **Calculated spot size as a function of wavelength for 84% encircled energy diameter from Equation 15 of Reference 10 using the full-scale aero-optical data from the present study.**